

Accepted Manuscript

Research paper

Synthesis, crystal structure, biomolecular interactions and anticancer properties of Ni(II), Cu(II) and Zn(II) complexes bearing S-allyldithiocarbazate

Nanjan Nanjundan, Ramaswamy Narayanasamy, Ray Jay Butcher, Jerry P. Jasinski, Krishnaswamy Velmurugan, RajuNandhakumar, Manickam Dakshinamoorthi Balakumaran, Pudupalayam Thangavelu Kalaichelvan, Vettaikaranpudur G. Gnanasoundari

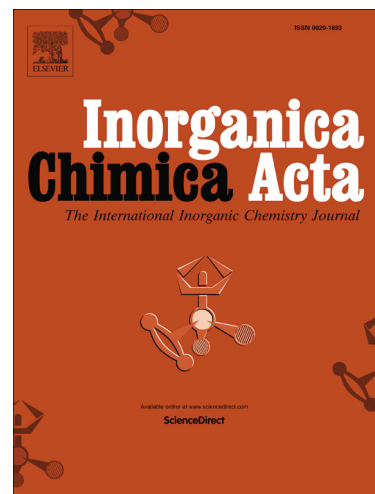
PII: S0020-1693(16)30758-7
DOI: <http://dx.doi.org/10.1016/j.ica.2016.10.035>
Reference: ICA 17328

To appear in: *Inorganica Chimica Acta*

Received Date: 18 June 2016
Revised Date: 27 September 2016
Accepted Date: 23 October 2016

Please cite this article as: N. Nanjundan, R. Narayanasamy, R. Jay Butcher, J.P. Jasinski, K. Velmurugan, RajuNandhakumar, M. Dakshinamoorthi Balakumaran, P. Thangavelu Kalaichelvan, V.G. Gnanasoundari, Synthesis, crystal structure, biomolecular interactions and anticancer properties of Ni(II), Cu(II) and Zn(II) complexes bearing S-allyldithiocarbazate, *Inorganica Chimica Acta* (2016), doi: <http://dx.doi.org/10.1016/j.ica.2016.10.035>

This is a PDF file of an unedited manuscript that has been accepted for publication. As a service to our customers we are providing this early version of the manuscript. The manuscript will undergo copyediting, typesetting, and review of the resulting proof before it is published in its final form. Please note that during the production process errors may be discovered which could affect the content, and all legal disclaimers that apply to the journal pertain.



Synthesis, crystal structure, biomolecular interactions and anticancer properties of Ni(II), Cu(II) and Zn(II) complexes bearing S-allyldithiocarbazate

Nanjan Nanjundan^a, Ramaswamy Narayanasamy*^a, Ray Jay Butcher^b, Jerry P. Jasinski^c, Krishnaswamy Velmurugan^d, RajuNandhakumar^e, Manickam Dakshinamoorthi Balakumaran^f, Pudupalayam Thangavelu Kalaichelvan^g, Vettaikaranpudur G. Gnanasoundari^h

^a*Department of Chemistry, Coimbatore Institute of Technology, Coimbatore-641 014, India.*

^b*Department of Inorganic and Structural Chemistry, Howard University, Washington DC 20059.*

^c*Department of Chemistry, Keene State College, Keene, NH 03435-2001, USA.*

^{d,e}*Department of Chemistry, Karunya University, Karunya Nagar, Coimbatore - 641 114, India.*

^{f,g}*Centre for Advanced Studies in Botany, School of Life Sciences, University of Madras, Guindy Campus, Chennai - 600 025, India.*

^h*Department of Chemistry, CBM college of Arts and Science college, Coimbatore – 641042, India.*

*To whom correspondence should be addressed, e-mail: narayanasamycit@gmail.com

Fax: + 91-422-2575020.

Abstract

A new series of bivalent Ni(II), Cu(II) and Zn(II) metal complexes containing Schiff base ligand [**H-emk-sadtc**] [(E)-allyl 2-(butan-2-ylidene) hydrazine carbodithioate] were synthesized and characterized by different spectroscopic techniques. The molecular structure of the ligand and its complexes **1** [(E)-allyl 2-(butan-2-ylidene) hydrazine carbodithioato nickel(II)], complex **2** [(E)-allyl 2-(butan-2-ylidene) hydrazine carbodithioato copper(II)], complex **3** [(E)-allyl 2-(butan-2-ylidene) hydrazine carbodithioato zinc(II)] were confirmed by single crystal X-ray crystallography. XRD data of the complexes had revealed a distorted square planar geometry around the metal ion, satisfied by N₂S₂ fashion. Density functional calculations of all the compounds in gas phase were performed by using DFT (B3LYP) with 6-311G basis set. The calculated FT-IR and structural data are in good agreement with the experimental results and confirmed by the experimental one. The interactions of calf thymus (CT) DNA and bovine serum albumin (BSA) with complexes **1-3** were explored by emission spectra. Catecholase and Phosphatase-like activities of all the complexes were also investigated. An *in vitro* cytotoxicity study of the complexes had shown significant activity against human cervical cancer cell line (HeLa) with the best results of complex **2**, which was found to be more toxic to cancer cells with a few micromolar concentrations, as the IC₅₀ value, but significantly less toxic to normal cell lines. Additionally, the cell death analysis was carried out by AO/EB and DAPI staining methods.

Key words: S- allyl dithiocarbamate, Ni(II), Cu(II) and Zn(II) complexes, Single crystal Study, Biomolecular interaction, Catalytic activity

1. Introduction

Developments of coordination chemistry of transition metal complexes have gained significant importance because of their fascinating structures and enormous potential applications in pharmacy, biochemistry, industry and so on. During the last few decades, Schiff base metal complexes have been extensively studied. Schiff bases are an interesting group of organic compounds, having an azomethine linkage (C=N) and are very useful due to their stability, chelating properties and biological applications. Various transition metal complexes of Schiff bases derived from the dithiocarbazate compounds, containing nitrogen, sulphur and/or oxygen as ligand atoms have been found to display a variety of pharmacological properties [1-3]. In recent years, study of dithiocarbazate-derived Schiff base metal complexes has received much attention [4-6]. Apart from studying different biological processes induced by metal ions, many new molecules have also been developed over the years, showing interesting properties. Whereas, the transition metal ions perform a pivotal role in terms of structural organisation and overall functionality.

In the field of nickel, copper and zinc complexes acting as DNA targeting drugs and anticarcinogens, the complexes derived from dithiocarbazate ligands played increasingly important roles, because of the strong coordination ability with metals, resulting in favorable interaction with DNA, mainly including intercalation and groove binding. On the other hand, Bovine serum albumins (BSA) are most extensively studied, as they play important role in bio-regulatory functions like maintenance of colloidal osmotic blood pressure, blood pH and the deposition of a wide variety of endogenous and exogenous substances in blood. Further BSA studies are useful for their effective role in drug delivery and binding properties with transition metal complexes.

Catalytic properties of dithiocarbazate Schiff base metal complexes have been rarely investigated. Moreover, the coordination compounds of nickel(II), copper(II) and zinc(II) with Schiff base ligands have been widely studied because, such complexes play an important role in redox enzyme systems and may provide the basis of models for active sites of biological systems or can act as catalysts [7-13]. As expected from their hard/soft nature, Schiff base ligands have found their principal applications in oxidation/reductive reactions, as well as catalysts for hydrolysis reactions [14,15]. Recently, we have reported the synthesis and X-ray structures of

new distorted tetrahedral nickel(II), copper(II) and zinc(II) complexes with Acetophenone appended Schiff base ligand.

As a continuation of our research work neutral mononuclear Ni(II), Cu(II) and Zn(II) complexes with the ligand (H-emk-sadtc = Ethyl methyl ketone with S-allyldithiocarbazate) of general formulae **1** Ni[(H-emk-sadtc)₂], **2** Cu[(H-emk-sadtc)₂] and **3** Zn[(H-emk-sadtc)₂] were synthesized and characterized. All these compounds were structurally characterized by single crystal X-ray diffractometry. The interaction of complexes **1-3** with CT-DNA and BSA were studied using fluorescence spectroscopy. Furthermore, compound **2** showed interesting catalytic activity towards catechol oxidation and phosphate hydrolysis as reported here. The anticancer activity of all the complexes was tested with HeLa cancer cell line. The mode of cell death was studied with AO/EB and DAPI staining assays.

2. Experimental

2.1. Materials and Instrumentation

All the reagents used in this study were of analytical grade and used without further purification. Solvents were purified and dried according to the standard procedures. Double distilled water was used to prepare buffers. Calf thymus DNA (CT-DNA), agarose, protein markers and Bovine serum albumin (BSA) were obtained from Genei, Bangalore and Himedia, India respectively. Ethidium bromide (EB), Methylene blue and Tris(hydroxymethyl) amino methane were purchased from Sigma-Aldrich and used as received.

Elemental analyses (C, H, N and S) were carried out on a Vario EL III CHNS analyzer. Infrared spectra were recorded (as KBr pellets) on Perkin-Elmer FT-IR spectrophotometer in the range of 4000-400 cm⁻¹. ¹H and ¹³C NMR spectra were recorded on Bruker Ultra Shield at 300 MHz, using CDCl₃ as a solvent and TMS as an internal reference. Mass spectra for the complexes were recorded on advanced Q-TOF Micro™ mass spectrometer, using electro spray ionization probe. Electronic spectra were obtained on JASCO V-570 Spectrophotometer. Fluorescence spectral data were performed on a JASCO FP-8200 fluorescence spectrophotometer at room temperature. Single crystal X-ray diffraction data collections were recorded at 173 K on a SHELXL-2014/7 diffractometer, equipped with liquid nitrogen cryostat. The melting points were checked on a Technico micro heating apparatus and were uncorrected. Stock solutions of M(II) complexes (1.0×10⁻³ M in DMSO) were stored at 4°C and the required

concentrations were prepared for all the experiments. All the stock solutions were used within four days. Solutions of the compounds were freshly prepared 1 hour prior to the biochemical evaluation. Data were expressed as the mean \pm standard deviation from three independent experiments.

2.2. Synthetic procedure for the ligand [**H-emk-sadtc**]

The ligand [**H-emk-sadtc**] was prepared according to literature procedure [16]. The light yellow precipitate was dissolved in acetonitrile/ethanol (70:30) mixture (20 mL) and kept for slow evaporation. After few days, light yellow needle-shaped single crystals isolated were washed with small amount of cold ethanol and pet-ether and dried in vacuum over anhydrous CaCl_2 .

Characterization data: Yield: 60-65%; Color: yellow; M.P: 150°C; Anal. Cal: $\text{C}_8\text{H}_{14}\text{N}_2\text{S}_2$; Calculated: C, 47.49; H, 6.97; N, 13.84; S, 31.69. Obtained: C, 46.94; H, 6.84; N, 13.79; S, 31.74; UV-Vis (DMSO), λ_{max} (nm): 276, 368. FT-IR (vcm^{-1} , KBr): 1635 $\nu(\text{C}=\text{N})$; 1033 $\nu(\text{C}=\text{S})$; ^1H NMR (CDCl_3 , 25°C, ppm): 9.87 (s, 1H, NH), 2.33 (s, 2H, CH_2), 1.14- 2.35 (s, 3H, CH_3), 3.95 (s, 2H, S- CH_2), 1.96 (s, H, CH); ^{13}C NMR (CDCl_3 , 25°C, ppm): 199.3 (C=S), 157.55 (C=N), 37.7 (S- CH_2), 77.10 (C- CH_2), 32.53 (CH- CH_3), 16.5 (CH_3), 118.9 (CH= CH_2).ESI-MS (Calcd, found, m/z) = 202.3, 202.03.

2.3. Synthesis of the Complex **1** $\text{Ni}[(\text{H-emk-sadtc})_2]$

Nickel(II) acetate tetrahydrate (0.248 g, 1 mmol) in 20 mL of ethanol and the ligand [**H-emk-sadtc**] (0.404 g, 2 mmol) in 20 mL of hot ethanol was added dropwise, the colour changes from light green to brown. The volume of the solution was reduced to 15 mL and kept for slow evaporation. Dark brown square-shaped single crystals were obtained after one week. The crystals were washed with ethanol and pet-ether and dried in vacuum over anhydrous CaCl_2 . Characterization data: Yield: 80-85%; Color: Dark brown; M.P: 155°C; Anal. Cal: $\text{C}_{16}\text{H}_{26}\text{N}_4\text{NiS}_4$; Calculated: C, 41.65; H, 5.68; N, 12.14; S, 27.80. Obtained: C, 40.64; H, 5.58; N, 11.89; S, 27.74; UV-Vis (DMSO), λ_{max} (nm): 368, 396, 456, 507. FT-IR (vcm^{-1} , KBr): 1589 $\nu(\text{C}=\text{N})$; ^1H NMR (CDCl_3 , 25°C, ppm): 2.95 (s, 2H, CH_2), 1.10- 1.50 (s, 3H, CH_3), 3.97 (s, 2H, S- CH_2), 3.01 (s, H, CH); ^{13}C NMR (CDCl_3 , 25°C, ppm): 170.07 (C-S), 37.65 (S- CH_2), 77.48 (C- CH_2), 28.54 (CH- CH_3), 14.47 (CH_3), 118.2 (CH= CH_2).ESI-MS (Calcd, found(M+H)⁺, m/z) = 461.36, 462.94

2.4. Synthesis of the Complex **2** Cu[(H-emk-sadtc)₂]

A hot ethanolic solution of ligand [**H-emk-sadtc**] (0.404 g, 2 mmol) in 20 mL was added to copper(II) acetate monohydrate (0.199 g, 1 mmol) in 20 mL of chloroform and the solution was allowed to reduce to 15 mL on a water bath at 50⁰C. The resulted brownish black solution was cooled and filtered. The filtered solution was kept for slow evaporation at room temperature. After 10 days, brownish - black single crystals were collected by filtration, washed with chloroform/ethanol mixture (50:50) and dried over CaCl₂.

Characterization data: Yield: 80-85%; Color: Brownish black; M.P: 155⁰C; Anal. Cal: C₁₆H₂₆CuN₄S₄; Calculated: C, 41.22; H, 5.62; N, 12.02; S, 27.51. Obtained: C, 40.84; H, 5.48; N, 11.92; S, 27.64; UV-Vis (DMSO), λ_{max} (nm): 363, 389, 406, 624. FT-IR (vcm⁻¹, KBr): 1604 ν(C=N).ESI-MS (Calcd, found, m/z) = 466.21, 466.93.

2.5. Synthesis of the Complex **3** Zn[(H-emk-sadtc)₂]

Zinc(II) acetate dihydrate (0.219 g, 1 mmol) dissolved in 20 mL of methanol was added to the ligand [H-emk-sadtc] solution (0.404 g, 2 mmol) of 20 mL of acetonitrile with constant stirring for 10 minutes. Then, the resulting mixture was refluxed on a water bath for 30 mins and reduced upto 15 mL, cooled and filtered. The filtrate was kept in refrigerator over a period of 15 days and the yellow colored needle - shaped crystals were isolated from the mother liquor and dried in CaCl₂ desiccator.

Characterization data: Yield 70%; Color; Yellow; M.P: 176⁰C; Anal. Formula: C₁₆H₂₆N₄S₄Zn
Calculated: C, 41.06; H, 5.60; N, 11.97; S, 27.40; Obtained: C, 41.28; H, 5.41; N, 10.98; S, 22.59; UV-Vis (Tris-HCL buffer), λ_{max} (nm): 236, 341. FT-IR (vcm⁻¹, KBr): 1612 ν(C=N); ¹H NMR (CDCl₃, 25 ⁰C, ppm): 2.32 (s, 2H, CH₂), 1.06- 2.31 (s, 3H, CH₃), 3.82 (s, 2H, S-CH₂), 2.43 (s, H, CH); ¹³C NMR (CDCl₃, 25 ⁰C, ppm): 177.91 (C-S), 177.23 (C-N), 35.53 (S-CH₂), 77.22 (C-CH₂), 33.43 (CH-CH₃), 19.76 (CH₃), 117.9 (CH=CH₂).

2.6. Crystallographic measurements

Crystals of the ligand [**H-emk-sadtc**] and its complexes **1-3** of suitable size selected from the mother liquor were mounted on the tip of a glass fiber and cemented using epoxy resin. The crystallographic data for all the compounds were collected on a SHELXL-2014/7 diffractometer equipped with a CCD-area detector on Oxford Diffraction X-Calibur Eos Gemini System. X-ray radiation employed was generated from a Mo sealed X-ray tube (Kα = 0.70173 Å), fitted with a

graphite monochromator. Data analysis was carried out using CrysAlis program. Unit-cell dimensions and intensity data for all the compounds were measured at 173(2) K. The unit cell was verified by the examination of h k l overlays on several frames of data by comparing with both the orientation matrices. After careful examination of the unit cell, a standard data collection procedure was initiated using omega scans. All the non-hydrogen atoms were refined with anisotropic thermal parameters. The structure was refined (weighted least squares refinement on F^2) to convergence. Absorption corrections were carried out using multi-scan method. The MERCURY was employed for the final data presentation and structure plots. Crystal data and additional details of data collection and refinement of the structures are presented in **Table 1**.

Insert Table 1

2.7. Theoretical calculations

All the computational calculations were performed with Gaussian 09 program using Density Functional Theory (DFT) with a combination of 6-311G basis set [19]. The initial coordinates obtained from the crystal structure of the ligand and its complexes were used for optimization. Visualization of the DFT optimized structures and frontier molecular orbitals (HOMO and LUMO) of the ligand and its complexes **1-3** were performed with the chemcraft program package (<http://www.chemcraftprog.com>). The vibrational frequency calculations were performed to ensure the optimized geometries that represent local minima on the potential energy surface with only positive eigen-values. The minimum energy structures were ensured by the absence of any imaginary frequency. Also, the theoretical investigation of the natural charge for each atom and QM descriptors were calculated using the same basic set.

2.8. DNA and EB-DNA binding experiments

DNA and EB-DNA binding experimental studies were carried out by employing the procedure reported by us previously [16].

2.9. Tryptophan fluorescence quenching experiments

Tryptophan fluorescence quenching studies were carried out as described previously [20].

2.10. Catalytic oxidation of 3,5-DTBC

A study of catecholase activity was performed by the widely used 3,5-di-tert-butylcatechol (3,5-DTBC) as the substrate, because its low redox potential makes it easily oxidized to the corresponding quinone (3,5-DTBQ) [21]. Since, it prevents over oxidation reaction, such as ring opening because of its highly stability, it shows a maximum emission at 435 nm in pure DMSO. The increase in emission at 435 nm with the increased oxidized species of 3,5-tert-butyl benzoquinone showed that the complexes **1-3** were oxidized 3,5-DTBC effectively under the same reaction conditions. Hence, a detailed kinetic study of DTBC was performed, before we started to evaluate the catalytic ability of the complexes **1-3** to oxidize 3,5-DTBC to 3,5-DTBQ at room temperature in oxygen atmospheric condition (**Scheme 1**).

Insert Scheme 1

For this purpose, 10^{-4} M DMSO solutions of the metal complexes were treated with 10^{-2} M (100 equivalents) 3,5-DTBC. Maintaining the concentration of the complex as constant and by adding different substrate concentrations ($10 - 50 \times 10^{-2}$ M), the immediate reaction progress was monitored by the fluorescence spectrometer at 15 minutes time interval over the reaction period of 2 hours, which was indicative of the formation of the corresponding quinone 3,5-DTBQ and was analyzed by Michaelis–Menten equation, as well as, Lineweaver–Burk plot (**Fig. 5**), which provided a turnover number.

2.11. Phosphatase hydrolysis activity

In order to study the hydrolytic activity of the complexes **1-3**, (10^{-4} M) solutions in pure dimethyl sulphoxide (DMSO) were treated with 100 equiv (10^{-2} M) of disodium (4-nitrophenyl) phosphate hexahydrate (4-NPP) under aerobic conditions at the room temperature (**Scheme 2**).

Insert Scheme 2

To determine the dependence of rate on the substrate concentrations and various kinetic parameters, (10^{-4} M) solution of the complexes **1-3** were treated with 10, 20, 30, 40, 50 and 60 equivalents of the substrate. The emission versus wavelength scans of the solution was recorded at regular time interval of 15 min in the wavelength range of 350-650 nm. The reaction was

followed spectrophotometrically by monitoring the increase in emission at 485 nm (4-NP band maximum) as a function of time as depicted in **Fig 6**. From this figure, it is evident that the observed spectral changes upon the addition of complexes **1-3** with increasing concentration of 4-NPP demonstrates active hydrolysis reaction. The dependency of rate on the concentration of substrate was analyzed by the Michaelis–Menten approach of enzymatic kinetics to obtain Lineweaver–Burk plot and the values of kinetic parameters, V_{\max} , K_M , and K_{cat} [23,24].

2.12. Antiproliferative activity

2.12.1. Cell culture

The human cervical cancer cell line (HeLa) was obtained from the National Center for Cell Science (NCCS), Pune, India. The cells were cultured in RPMI 1640 medium (Biochrom AG, Berlin, Germany), supplemented with 10% fetal bovine serum (Sigma), cisplatin (Getwell pharmaceuticals, India), and 100 $\mu\text{g}/\text{mL}$ penicillin and 100 $\mu\text{g}/\text{mL}$ streptomycin, as antibiotics (Himedia, Mumbai, India) in 96-well culture plates at 37°C under a humidified atmosphere of 2% CO_2 in a CO_2 incubator (Heraeus, Hanau, Germany). All the experiments were performed using cells from the passage 15 or less.

2.12.2. Cell viability assay

The *in vitro* growth inhibitory effect of the complexes **1-3** towards tumour cell line was evaluated by the MTT (tetrazolium salt reduction) assay on the human cervical cancer cell line (HeLa) and normal Vero cell line. Cell viability was carried out using MTT assay method as prescribed previously [25, 26]. The complexes **1-3** in the concentration range of 10-100 μM were dissolved in DMSO and in all the experiments, the percentage of DMSO was maintained in the range of 0.1-1%. DMSO by itself was found to be non-toxic to the cells upto 1% concentration. After 24 h, the medium was replaced with respective medium of 1% FBS containing the compounds at various concentrations and incubated at 37 °C under the conditions of 5% CO_2 , 95% air and 100% relative humidity for 24 h. After 24 h, 10 μL of MTT (5 mg mL^{-1}) in phosphate buffered saline (PBS) was added to each well and the plates were wrapped with aluminum foil and incubated at 37 °C for 4 h. The medium with MTT was then discarded and the formed formazan crystals were dissolved in 100 μL of DMSO. The absorbance was monitored at 570 (measurement) and 630 nm (reference) using a 96-well plate reader (Bio-Rad, Hercules, CA) to 50% of those in the untreated control wells and a graph was plotted with the percentage of cell

inhibition *versus* concentration. Data were collected for three replicates each, and used to calculate the mean. The percentage inhibition was calculated from this data, using the formula [27, 28].

$$\text{Inhibition rate (IR \%)} = \frac{\text{OD (control)} - \text{OD Drug treated cells}}{\text{OD (control)}} \times 100$$

The corresponding IC_{50} (concentration of drug that inhibits cell growth by 50%) value was determined by the nonlinear regression analysis using Origin 6.0 software.

3. Results and Discussion

3.1. Synthesis and characterization

Three new mononuclear complexes were synthesized from straight forward reactions of the ligand mixed with metal acetates in 2:1 ligand: metal ratio. Complexes **1-3** were obtained in good yields and found soluble in ethanol, methanol, chloroform, dichloromethane, DMSO and DMF. The complexes were stable at room temperature and analytically pure microanalytical data confirmed to the proposed molecular formula (data given in the Experimental section).

Insert Scheme 3

3.1.1. FT - IR spectra

The ligand has a proton adjacent to the thione group. It has been stated that the thione group [-NH-C(=S)-] is relatively unstable in monomeric form and tends to form a more stable C-S single bond by enethiolization, if there is at least one hydrogen atom adjacent to the thione ν (C=S) bond [29]. FT-IR spectral assignments for the ligand and its complexes **1-3** are listed in the experimental section and also in **Table S1**. FT-IR spectrum of the ligand does not exhibit a ν (S-H) band at around 2,500–2,700 cm^{-1} , suggesting that in the solid state, the thione form predominates [30]. The strong band at 3178.6 cm^{-1} of the free ligand is assigned to -NH and lack of this band in the complexes indicates that the nitrogen atom is deprotonated during coordination. This provides a strong evidence for the coordination of the ligand with M(II) ion in the thiolate form [31,32]. In addition, a strong band assigned to azomethine ν (C=N) vibration was observed at 1635 cm^{-1} in the spectra of the ligands that experienced a downward shift of 23-46 cm^{-1} , indicating the coordination of ligands to M(II) ion via azomethine nitrogen atom. The hydrazinic ν (N-N) stretching vibration band of free ligands at 1303.3 cm^{-1} is also shifted to the

higher region 70-116 cm^{-1} upon metal complexation, to further support the coordination of nitrogen atom to the metal centre. Another strong band at 1033.8 cm^{-1} for the free ligand is assigned to $\nu(\text{C}=\text{S})$, which is also disappeared in the complexes **1-3**, suggesting that the sulphur atom is coordinated through the metal centre in thiolate form [33]. The $\nu(\text{C}-\text{S}-\text{S})$ strong band of the uncoordinated free ligand at 956.6 cm^{-1} is also shifted to higher wave number at 23 cm^{-1} in the spectra of the respective complexes, coordinated via the thione/thiolate sulphur atom. A new band that is observed for the metal complexes at 586.3 cm^{-1} is attributed to $\nu(\text{M}-\text{N})$ and the complexes exhibit medium intensity band at 424.3 – 416.6 cm^{-1} , which may be assigned to $\nu(\text{M}-\text{S})$.

3.1.2. Emission Spectra

The electronic spectral data of the ligand showed bands at 222, 304 and 335 nm. The intensity of the band at 222 nm is due to ($\pi \rightarrow \pi^*$, $\text{CH}=\text{N}$) and 304 nm band for ($\pi \rightarrow \pi^*$, dithiocarbazate moiety). Complexes **1** and **2** possess similar characteristic spectral features that are depicted in **Fig S1**. The spectral data were summarized in the experimental section. The complexes exhibited intra-ligand transitions in the range of 360-397 nm, which are mostly due to non-bonding electrons ($n \rightarrow \pi^*$, dithiocarbazate moiety) present in the nitrogen atom of azomethine group in Schiff base complexes. In addition, the complexes showed bands at around 400 nm that might be assigned to $\text{S} \rightarrow \text{M}$ charge transfer transition, indicating the coordination of Schiff base to the metal atom via thiolate sulfur. While, Ni(II) and Cu(II) complexes (**1** and **2**) showed very broad weak $d-d$ band around 660-680 nm region attributed to distorted square planar geometry. The diamagnetic complexes showed absorption bands corresponding to ${}^1\text{A}_{1g} \rightarrow {}^1\text{A}_{2g}$, ${}^1\text{A}_{1g} \rightarrow {}^1\text{B}_{1g}$ and ${}^1\text{A}_{1g} \rightarrow {}^1\text{E}_g$ transitions [34]. The absorption observed for Zn(II) complex (**3**) is consistent with d^{10} metal ion configuration and shows no $d-d$ transitions as well.

3.1.3. ${}^1\text{H}$ NMR spectra

In the presence of transition metal ions, Schiff base ligands are converted into thiol tautomeric forms to facilitate the formation of centric neutral bis-ligand metal complexes. Both thiol sulfur and azomethine nitrogen, like other kinds of these ligands, coordinate to the metal atom. The spectra of free ligand and its complexes **1** and **3** showed well-defined signals that indicate no fluxionality in solution (**Fig. S4-S6**). The integration of the ${}^1\text{H}$ resonances confirms

that [H-emk-sadtc] ratio is in good agreement with the structural composition of *cis* complexes 1-3 (Fig. S4–S6). ^1H NMR data for the ligand and its corresponding complexes are summarized in the experimental section. The ligand shows signal at 9.87 ppm, which is assigned to N-H proton and it exists, predominantly as *E* form of the isomer [35]. The lack of this signal in complexes confirms that azomethine nitrogen is coordinated to the metal centre. This is inconsistent with the presence of thione form in solution [36]. For further confirmation, it is noted that ^1H NMR spectra of the ligand in CDCl_3 do not show any signal to S-H proton in solution, which is a strong evidence that it also remains solely in thione tautomeric form. In contrast, Schiff bases derived from S-alkyl/aryl dithiocarbazates have always been shown deprotonation, while coordinating to the metal ion, yielding complexes of deprotonated thiolate form of the ligand [37, 38]. The methylene protons, ligands and their complexes do not show any changes. It remains that S-benzyl/allyl sulphur do not take part in coordination.

3.1.4. ^{13}C NMR spectra

Due to paramagnetic nature of the complex **2**, ^1H and ^{13}C NMR spectra could not be studied. ^{13}C NMR spectra of the ligand and its complexes were recorded in CDCl_3 and the signals obtained are in good agreement with the probable structure. The ligand shows signals at 199.30 and 157.55 ppm, which are due to thioamide carbon (C=S) and azomethine carbon (C=N), respectively. The low intensity is due to the deshielding effect of nitrogen and two sulphur atoms, adjacent to carbon. These electronegative elements produce a large downfield shift, since they are directly attached to the carbon atom. In the complexes, (C=S) peak is shifted significantly upfield to maximum 13-22 ppm, as compared to the ligand, which confirms bonding through thione sulphur atom. However, comparison of ^{13}C NMR spectra of the ligand with that of the complexes **1** and **3** show that there is only a very little shift of the signals due to the azomethine and thioamide carbon atoms, indicating the fact that the coordination does not affect the electronic environment around those atoms, because of delocalization of electrons in the dithiocarbazate moiety (Fig. S7 – S9).

3.1.5. Description of Molecular structure [H-emk-sadtc]

The molecular structure of [H-emk-sadtc] with its atom numbering is shown in Fig. 1. The selected bond lengths and angles are listed in Table 2. Schiff base is obtained as

monoclinic crystals with a space group of $P2_1/n$. Schiff base is in thione form with C5=S1 bond distance 1.6603(17) is intermediate between a pure single bond ca. 1.81 Å and the double bond ca. 1.58 Å, possibly due to extensive conjugation over C5-N1-N2-C1 chain and other intermolecular interactions [39]. The N1-N2 distance, 1.3865(19) is similar to that found in S-benzylthiocarbamate [40] and S-methylthiocarbamate [41] although, a little but significant contraction of the bond may be attributed to the extension of a π -electronic system along with dithiocarbamate backbone [42]. The *cis-trans* isomerism is exhibited in Schiff base around thioamide moiety [43]. As observed that the ethyl methyl ketone chain is *trans* with respect to terminal thione S1 atom about the azomethine nitrogen atom N2, which is similar to the free, unsubstituted thiosemicarbazides and S-alkylthiocarbamates [44]. In contrast, S-allyl group is *cis* with respect to the terminal C5=S1 about the C5-S2 bond. The bond angles are approximately closer to 120° in consistent with sp^2 hybridization. Both ethyl methyl ketone and S-allyl moieties are not essentially planar, but exist with twisted conformations as shown from their dihedral angles.

Insert Fig. 1

The N2 - N1(H)-C5=S1 and N1(H)-C5-S2-C6 chains adopt *trans* conformation with torsion angles -178.67(12) [°] and -178.4(6) [°], respectively whereas, S1-C5-S2-C6 chain adopts *cis*-conformation about C1=N2 with torsion angle 1.7 [°] that shows *E* configuration. However, in solution, 180° rotations of the fragment S2-C5-S1 about C5-N1 bond orient two donor atoms N, S that are in the correct position for bidentate coordination.

3.1.6. Molecular structural characterization of complexes 1-3

Insert Fig.2

Crystal structures of complexes 1-3 reveal four - coordinate geometries with two symmetric Schiff bases bonded to the metal ions as shown in Fig. 2. In complexes 1-3, deprotonation of the ligand leads to tautomerization to the iminothiolate. In each case, the metal(II) center is coordinated by two N,S-bidentate ligand and exists within a *cis*-O2S2 donor set that defines a square planar geometry. While coordinating in iminothiolate form, the negative

charge generated on sulphur atom is delocalized in the C=N – N=C chain, as indicated by the intermediate C5-N2 bond lengths in complexes **1**(1.280), **2** (1.287, 1.277) and **3** (1.283, 1.291).

Insert Table 2

In all the complexes, M-N bond distances are comparably shorter than M-S distances. This indicates that the coordinated ligand is in thiolato form. The sum of the angles around metal centre for complexes **1-3** (364.4, 380.3, 409.60) indicate that complex **3** is more distorted than complexes **1** and **2** as a regular square planar geometry.

3.1.7. DFT geometrical analysis and calculations

The geometries of ligand and its complexes **1-3** were optimized using B3LYP/6-311G level of calculations in the singlet ground state. The input files were prepared from crystallographic coordinates obtained from X-ray measurements. The optimized structures of the compounds were depicted in **Fig. S13** and contour plots of the compounds were shown in **Fig S14**. The important calculated bond-lengths and bond-angles of all the compounds are in good agreement with experimentally observed single crystal X-ray data measurements as listed in **Table 2**. FT-IR spectroscopic analyzes were carried out to investigate vibrational responses of the functional groups of all compounds. The vibrational assignments of FT-IR intensities and normal mode descriptions of compounds are listed in the supplementary material (**Table S1**) and the obtained spectra of all compounds are given in **Fig S3**.

FT-IR spectrum of NH stretching band is usually observed above 3200 cm^{-1} . However, this band is shifted to lower frequency region due to intra- and inter-molecular hydrogen bonding by the NH band that is observed at 3178 cm^{-1} of the IR spectrum. From the computed frequencies, a strong peak at 3156 cm^{-1} corresponding to NH stretching vibration of the ligand is observed. The C=N band in free ligand occurred at 1695 cm^{-1} , upon complexation, is shifted to 1535, 1538 cm^{-1} , which confirms the coordination of ligand through imine nitrogen. The absence of C=S band in complexes, is confirmed by the thiolic sulphur is coordinated to the metal ion. The theoretical calculations are strongly correlated with the experimental values and confirmed that the ligand is coordinated through N_2S_2 mode.

Since the experimental and theoretical data can be used for the identification of compounds, we have followed these data to confirm the structure of complexes. A difference

between experimental and theoretical studies is that the computations were done in gas phase while X-ray data were obtained in solid phase for all the compounds. While some calculated values are smaller than the experimental, some values are larger. Some of bond angles showed large deviations from experimental ones. In the free ligand C=N, C=S bond lengths of 1.359 and 1.707Å are elongated in complexes. The calculated geometry also proves distorted square planar geometry around metal atom.

The atomic charge distributions on donor–acceptor atoms for the complexes under investigation were obtained from NBO analysis. Electronegativity (χ), chemical potential (μ), global hardness (η), global softness (S) and electrophilicity index (ω) are global reactivity descriptors, which are highly successful in predicting global reactivity trends. On the basis of Koopmans's theorem [45], global reactivity descriptors are calculated from the energies of frontier molecular orbitals ϵ_{HOMO} , ϵ_{LUMO} as, listed in **Table S2**.

$$X = -1/2(\epsilon_{\text{HOMO}} + \epsilon_{\text{LUMO}})$$

$$\mu = -\chi = 1/2(\epsilon_{\text{HOMO}} + \epsilon_{\text{LUMO}})$$

$$\eta = 1/2(\epsilon_{\text{HOMO}} - \epsilon_{\text{LUMO}})$$

$$S = 1/2\eta$$

$$\omega = \mu^2 / 2\eta$$

Depending upon the value of electrophilicity index, the molecule can act as an electrophile or a nucleophile. Based on the above calculations, the electrophilicity index of the free ligand and its complexes are found to be 1.717, 2.293, 5.564 and 2.066 eV. Thus, the complex **2** comparably has higher global electrophilicity index (ω) and hence better is electrophilic character. The kinetic stability, chemical reactivity and color of the transition metal complexes in solutions are governed by HOMO–LUMO energy differences. The HOMO–LUMO energy gap of compounds are 4.513, 3.698, 1.836 and 3.516, where a ligand can be excited easily whereas, a higher energy gap results in higher kinetic stability, but lower chemical reactivity of the molecule. Further, the energy of HOMO is directly related to ionization potential and LUMO energy is directly related to electron affinity. Thus, greater the E_{HOMO} value greater will be, the electron donating capability and smaller the E_{LUMO} value will be smaller the resistance to accept electrons.

The net atomic charge for atoms of the title compound calculated by Natural Population Analysis (NPA) was presented in **Table S3**. The calculated charge value for nitrogen atoms are in contrast to the expected one (-1 a.u.), which indicates electron transfer from these atoms to

metal center. Furthermore, the decrease of formal charges of sulfur and chlorine from the expected values of -2 and -1 a.u. is a reason for the migration of electrons to metal centre. Compared to atomic charges it can be seen that electron charge density on metal atoms in their respective complexes has increased, i.e., before complexation, charge on metal cation is +2, and after complexation charge of metal atoms are 1.26330, 1.07996 and 1.48052 respectively. This indicates that the ligands transfer their negative charges to the respective metal ions upon complex formation.

3.2. Emission spectra titration and CT-DNA binding evaluation

DNA binding is an important parameter for the chemical and photo-induced DNA cleavage activity of metal complexes. Therefore, interaction of metal complexes with CT-DNA can be conveniently monitored by fluorescence spectroscopy and also the changes in emission and shift in wavelength maxima. Binding of complexes to DNA through intercalation generally leads to hypochromism and bathochromism of emission band. This shift is observed due to strong stacking interaction between aromatic chromophore of the ligand and base pairs of DNA. Minor groove binding of the complexes to DNA results in hyperchromism in absorption intensity, resulting in the unwinding of DNA double helix as well as, its unstacking and concomitant exposure of the bases.

Insert Fig. 3

The observed emission spectra of complexes in the presence and absence of CT-DNA exhibited a hypochromic shift, which indicates that there is interaction between the complexes and CT-DNA, which is an evidence for intercalative binding mode as depicted in **Fig. 3**. In order to quantify binding affinity between complexes **1-3** and CT-DNA, the binding constant (K_b) values are listed in **Table 3**. The complex **2** ($2.556 \times 10^5 \text{ M}^{-1}$) shows higher binding propensity compared to other complexes. All the complexes have shown binding affinity yielding (K_b) values ($\sim 10^5 \text{ M}^{-1}$) in the order of **2 > 1 > 3**.

3.3. Emission titration in the presence of Ethidium bromide

The fluorescence spectral method using Ethidium bromide (EB) as a reference was used to determine relative binding of complexes **1-3** in Tris-HCl buffer (pH=7.2) solution of EB/DNA mixture. Before starting measurements, the mixture was shaken up and recorded. EB

was non-emissive in Tris-HCl buffer (pH=7.2) but, in the presence of DNA, EB showed enhanced intensity due to intercalative binding to DNA. Fluorescence intensities at 605 nm (excited at 540 nm) were measured at different complex concentrations (10-50 μM). The relative binding tendency of metal complexes to CT-DNA was determined by the comparison of slope of the line in fluorescence intensity versus complex concentration. Stern-Volmer quenching constant, K_{sv} was calculated using the equation [46, 47]

$$I_0/I = 1 + K_{sv}[Q]$$

where, I_0 and I are fluorescence intensities of EB-DNA in the absence and presence of complex respectively. $[Q]$ is quencher concentration, K_{sv} is a linear Stern- Volmer quenching constant slope obtained from linear fit plot of I_0/I vs $[\text{complex}]$. Further, the apparent binding constant (K_{app}) was calculated from the following equation:

$$K_{EB} [\text{EB}] = K_{app} [\text{complex}]$$

where, the complex concentration was obtained from the value at a 50% reduction of fluorescence intensity of EB, $K_{EB} = 1.0 \times 10^7 \text{ M}^{-1}$ and $[\text{EB}] = 7.5 \mu\text{M}$.

Insert Fig. 4

3.4. Competitive interaction of the complexes with EB-DNA

To check whether the binding of complexes **1-3** with DNA is of the groove or intercalative nature, we have performed a comparative binding study with EB by adding the complexes as quenchers. EB is a planar cationic dye that can intercalate to CT-DNA and soluble complexes with nucleic acids. EB in buffer medium with stacking shows interaction of planar phenanthridium ring between the adjacent base pairs [48, 49]. The enormous quenching in the emission intensity of EB in the DNA environment can be rationalized by considering the intercalative binding of EB with DNA [50].

The emission spectra of DNA bound EB in the presence of varying concentrations of the complex is shown in (**Fig. 4**). The plot illustrates that the quenching EB bound DNA with complexes are in good agreement with linear Stern-Volmer equation [51, 52]. Stern-Volmer quenching constant (K_{SV}) $2.3\text{-}3.2 \times 10^5 \text{ M}^{-1}$ and the apparent binding constant (K_{app}) $1.59\text{-}1.74 \times 10^5 \text{ M}^{-1}$ values are listed in **Table 3**.

Insert Table 3**3.5. Tryptophan Quenching Experiments**

Serum albumin is the most abundant protein in the circulatory system. The most important physiological function of serum albumin is to maintain osmotic pressure, pH of blood and transport a wide variety of endogenous and exogenous compounds, including fatty acids, metal, amino acids, steroids and drugs. Because of these extraordinary characteristics, albumins from the various sources have gained extensive biomedical and industrial applications, as well as, research interest [53]. Fluorescence spectroscopy is an effective method to examine interaction between metal complexes and BSA. Here, we have investigated the binding affinity of complexes **1–3** with BSA under physiological conditions.

Insert Fig. 5

Fig. 5 shows the effect of increasing concentrations of the added complexes **1-3**, on fluorescence emission of BSA. The intensity of broad emission band at 342 nm decreases largely with the increasing concentration of complexes, which confirmed the fact that the interaction between the complexes and BSA have occurred.

Insert Fig. 6

The extent of quenching of fluorescence intensity, as expressed by the value of Stern-Volmer constant (K_{SV}), is a measure of protein binding affinity of the complexes. It is calculated from the equation [54, 55].

$$F_0/F = 1 + K_{SV}[Q]$$

where, F_0 and F are steady-state fluorescence intensities in the absence and presence of quencher, respectively. K_{SV} is Stern-Volmer quenching constant and $[Q]$ is the concentration quencher. The plot of F_0/F vs $[Q]$ (**Fig.6**) shows the value of K_{SV} . According to the equation.

$$K_{SV} = K_q\tau_0$$

where, K_q is quenching rate constant and τ_0 is fluorescence life - time of protein in the absence of quencher and the value of τ_0 is considered to be 10^{-8} s. K_{SV} and K_q values are obtained from the binding of complexes **1-3** with BSA as listed in **Table 4**. The values of quenching rate constant

(K_q) is 1000 times higher than optical collision rate constant, $2 \times 10^{10} \text{ M}^{-1}$ [56]. These results suggest that all the complexes interact strongly with BSA and the probable quenching mechanism is not initiated by dynamic quenching, but by a static one.

3.6. Binding Analysis

When the small molecules bind independently to a set of equivalent sites on a macromolecule, the equilibrium between free and bound molecules is given by Scatchard equation [57, 58].

$$\log (F_0 - F)/F = \log K + n \log [Q]$$

Where, K and 'n' are the binding constant and number of binding sites, respectively. The plot of $\text{Log } [F_0 - F]/F$ versus $\log [Q]$ (**Fig. 5.**) can be used to determine the values of both K as well as, 'n' and such values are calculated for the complexes, **1-3** and listed in **Table 4**.

Insert Table 4

The values of 'n' are approximately equal to 1, indicating that there is one class of binding site to complex in BSA. Fluorescence spectral results clearly show that the complexes are having the binding constant values that follows the order **2>1>3**. The higher binding affinity of **2** is enhanced due to copper metal centre and the efficacy may be increased by the phenyl group.

3.7. Kinetic Studies for Catecholase Activity

Proteins are the most important building blocks of a living cell. The entire collection of proteins of a living cell is also called as proteome. Metalloproteins containing Cu perform four basic functions: i) metal ion storage, transport and uptake ii) electron transfer iii) dioxygen storage, transport and uptake and iv) catalysis.

Insert Fig. 7

Catechol oxidase is a type III copper protein, containing a binuclear active site actively involved in the oxidation of catechols to the highly reactive quinones that undergo auto-polymerization and transform into a brown pigment, melanin. Moreover, the oxidation product, 3,5-DTBQ is highly stable and a characteristic emission band is appeared at 435 nm in pure

DMSO solvent system. Before going into the detailed kinetics, we have examined the 3,5-DTBC to the corresponding 3,5-DTBQ in DMSO solvent. We have observed that by using the complexes as catalyst and treated with 100 equivalents of 3,5-DTBC at room temperature under aerobic conditions. The progress of the reaction is followed by recording fluorescence spectra of the mixture at 15 minutes time interval. The gradual increase of an emission band corresponds to quinone.

In each cases, first-order kinetics is observed at a lower concentrations of 3,5-DTBC, whereas, higher concentrations led to the saturation kinetics (**Fig. S15**). The observed rate versus concentration of the substrate data are then analyzed on the basis of Michaelis–Menten approach of enzymatic kinetics to get Lineweaver–Burk (double reciprocal) plot and the values of kinetic parameters, V_{\max} , K_M , and K_{cat} . The curves of observed rate vs [substrate] and Lineweaver–Burk plots for complexes **1-3** are shown in **Fig. 7**.

$$1/V = \{ KM/V_{\max}\} \{1/[S]\} + 1/V_{\max}$$

The various kinetic parameters, such as Michaelis-Menten constant, K_{cat} (in 10^{-4} h^{-1}), maximum velocity V_{\max} and Michaelis binding constant (K_M) for complexes **1-3** are shown in **Table 5**. These results clearly show the ability of complex **2** to effectively catalyze 3,5-DTBC.

Insert Table 5

3.8. Phosphate Ester Cleavage Study and Kinetics

There are many reports cited in literature in which, the labile coordination site of mononuclear transition metal complexes assist the hydrolysis/ transesterification of phosphate esters. To study Phosphatase activity of complexes **1-3**, a disodium salt of (4-nitrophenyl)-phosphate hexahydrate was chosen as substrate. The catalytic efficiency of these complexes was determined by the method of pseudo first-order rate constant (k_{obs}) by monitoring the growth of 4-nitrophenolate emission band (485 nm), as a function of time. Their hydrolytic tendency was detected spectrophotometrically by monitoring time evolution of p-nitrophenolate anion (4-NP), through a wavelength scan from 350 to 650 nm in pure DMSO. After the addition of substrate to solutions of complexes **1-3**, the immediate spectral change corresponding to 4-NP anion for all the complexes showed promising catalytic activity towards 4-NPP. The course of a typical reaction with complexes **1-3** is shown in **Fig. 8**.

Insert Fig. 8

Initially, a first-order dependence of substrate concentration was observed (**Fig. S16**). At higher concentrations, saturation kinetics was found and first-order rate kinetics was gradually deviated from unity for all the active complexes. The dependence of rate on the substrate concentration had suggested a catalyst–substrate binding to be an initial step in the catalytic mechanism. A treatment on the basis of Michaelis–Menten approach, originally developed for enzyme kinetics was, therefore, applied and linearized by means of Lineweaver–Burk plot (**Fig. 8**.) to calculate various kinetic parameters, such as Michaelis–Menten constant (K_M) and maximum initial rate (V_{max}).

Insert Table 6

K_{cat} values can be calculated by dividing V_{max} values by the concentration of the corresponding complexes. These calculations are same as catecholase oxidation. The data obtained from Lineweaver–Burk plot model were used for the comparison of catalytic activity towards the hydrolysis of 4-NPP, as shown in **Table 6**. It might be stated that the complex **2** belong to the highly efficient catalyst group, where order of their activity is **2>1>3**.

3.9. Cytotoxicity in HeLa cells

3.9.1. MTT assay

Cytotoxicity of the complexes **1-3** was tested against human cervical cancer cell line (HeLa) and normal Vero cell line using 3-(4,5-dimethylthiazol-2-yl)-2,5-diphenyltetrazolium bromide (MTT) assay. Cisplatin was used as reference compound to evaluate the cytotoxic activity.

For the cytotoxic activity, different concentrations of the complexes, 10 -100 μ M were tested in triplicate for 48 h in two independent experiments. The results were expressed as the average \pm standard deviation of two independent experiments. From the percentage cell growth inhibition *versus* complex concentration plot, a dose-dependent cell death inducing the ability of complexes has been observed. This indicates that the metal ion does play a role in the observed cytotoxicity of metal complexes. All the complexes are active against the tested cell lines, but do not show any damage to normal cells with respect to the standard drug cisplatin.

When compared to inhibitory effect with respect to IC₅₀ values, complex **2** showed higher activity than other complexes (**Table 7**). Also, the cytotoxicity of complexes **1-3** follows the order **2>1>3**, which is consistent with the strong DNA binding of the complexes.

Insert Table 7

3.9.2. Dual-staining Assay

In order to assess the type of cell death induced by complexes in HeLa cells, the morphological changes after double staining with Acridine Orange–Ethidium Bromide (AO–EB) were investigated by fluorescence microscopy (**Fig. 9**). Four types of cytological changes were observed from fluorescence emission and the morphological features of chromatin condensation in AO/EB stained nuclei [59, 60]. (i) viable cells having uniform green fluorescing nuclei with highly organized structure; (ii) early apoptotic cells (which still have intact membranes, but have started undergoing DNA fragmentation) having green fluorescing nuclei, but peri-nuclear chromatin condensation is visible as bright green patches or fragments; (iii) late apoptotic cells having orange to red fluorescing nuclei with condensed or fragmented chromatin; and (iv) necrotic cells, swollen to large sizes, having uniformly orange to red fluorescing nuclei with no indication of chromatin fragmentation. These morphological changes are observed for complex **2**, which suggested the fact that the cells are committed to more efficient apoptotic cell death [61]. The mechanism of action is still not completely elucidated. Efforts are on to establish the mechanism of action. Inhibition of cancer cells and induction of apoptosis might be the efficient ways of treating cancer. Apoptosis eliminates cells, exposing the organism to danger. For example, virally infected cells or cells with damaged DNA will be removed by apoptosis [62]. In several proposed mechanisms, the two important types of apoptosis are: death receptor–dependent pathway, also called as extrinsic pathway and mitochondrial–dependent or intrinsic pathway. The positively charged metal complexes have the potential to act as effective metal-based anticancer drugs.

3.9.3. DAPI staining

To understand nuclear morphology and to determine cell death mechanism, DAPI staining test was carried out for its complexes **1-3**. Chromatin condensation during the process of

apoptosis (Type I programmed cell death) is a characterizing marker of nuclear alteration. HeLa cells were treated with 50 μ M concentration of the complexes **1-3**. The cells were incubated for 24 h before DAPI nuclear staining. Cells were examined under fluorescent microscope, fitted with a DAPI filter. Control cells (treated with 10% (v/v) DMSO) hardly showed sort of condensation in comparison with the treated cells, as shown in (Fig. 10).

Insert Fig. 9

After cell fixation, apoptotic nuclei were identified by the reduced nuclear size and gathering of condensed chromatin at the periphery of nuclear membrane, besides, the fragmented morphology of nuclear bodies. Furthermore, the normal cells are of uniform morphology without any nuclear condensation. The result clearly shows that as the concentration of the metal complex increases, the percentage of cells undergoing apoptosis also increases. Besides showing nuclear change, the treated cells exhibited a shrinking morphology, which is another important hallmark of apoptosis.

4. Conclusion

Three important potentially new anticancerous complexes derived from S-allyldithiocarbamate derivative had been synthesized and characterized. The characterization of the complexes was accomplished by elemental analyses and various spectral techniques. The solid state structure of the ligand and complexes **1-3** were confirmed by single-crystal X-ray crystallography. The binding behaviour of complexes **1-3** with DNA had revealed the existence of intercalative mode of interaction. From the results of fluorescence quenching experiments of BSA, it is concluded that the complexes have strong binding affinity in the static mode. Furthermore, the complexes had shown effective bio - catalytic activity for the oxidation of 3,5-DTBC and hydrolysis of 4-NPP. In addition, the complexes had shown widespread anti-tumor potency with low IC_{50} values tested by MTT assay against normal Vero cell line and HeLa cancer cell line. In particular, complex **2** exhibited comparatively higher cytotoxicity than other complexes. Finally, the characteristics of apoptosis in cell morphology have been observed using AO/EB and DAPI staining. The results obtained from the present compounds are of importance for the development of metal-based agents for anti-cancer applications in the future.

Acknowledgement

We are sincerely thankful to the SAIF Punjab University, Chandigarh for ESI mass facility and The Director, CAS in Botany, School of Life Sciences, University of Madras for providing laboratory facilities to perform the cell line studies. JPJ acknowledges the NSF-MRI program (Grant No.CHE-1039027) for funds to purchase the X-ray diffractometer.

Electronic supplementary information (ESI) available

UV Spectra of compounds (Fig S1), FTIR Spectra of compounds (Fig S2-S3), ^1H NMR Spectra of compounds (Fig S4-S6), ^{13}C NMR Spectra of compounds (Fig S7-S9), ESI Mass Spectrum of compounds (Fig S10-S12), Optimized structures (Fig S13). FMO diagrams (Fig S14). Kinetic Plot (3,5-DTBC) Rate vs Concentration of complexes (Fig S15), Kinetic Plot (4-NPP) Rate vs Concentration of complexes (Fig S16), DFT and Experimental values of IR spectra (Table S1). Electronic properties of [H-emk-sadtc] and its complexes 1–3 in B3LYP/6-311G level (Table S2). Natural charge and electronic configuration (Table S3). CCDC reference numbers 1484684-1484687 for compounds.

References

- [1] F.N.F. How, K.A. Crouse, M.I.M. Tahir, M.T.H. Tarafder, A.R. Cowley, *Polyhedron*. 27 (2008) 3325.
- [2] T.B.S.A. Ravoof, K.A. Crouse, M.I.M. Tahir, A.R. Cowley, M.A. Ali, *Polyhedron*. 26 (2007) 1159.
- [3] A. Garoufis, S.K. Hadjikakou, N. Hadjiliadis, *Coord. Chem. Rev.* 253 (2009) 1384.
- [4] M. Yazdanbakhsh, R. Takjoo, *Struct. Chem.* 19 (2008) 895.
- [5] A.N. Montenegro, R. Carballo, E.R.V. Lopez, *Polyhedron*. 27 (2008) 2867.
- [6] M.T.H. Tarafder, A.M. Ali, Y.W. Wong, S.I. Wong, K.A. Crouse, *Synth. React. Inorg. Met- Org. Chem.* 31 (2001) 115.
- [7] M.S. Sigman, E.N. Jacobsen, *J. Am. Chem. Soc.* 120 (1998) 4901.
- [8] P.G. Cozzi, *Chem. Soc. Rev.* 33 (2004) 410.
- [9] B.N. Shelimov, *Russ. Khim. Zh.* 44 (2000) 57.
- [10] K.C. Gupta, A.K. Sutar, *Coord. Chem. Rev.* 252 (2008) 1420.
- [11] T. Katsuki, *Chem. Soc. Rev.* 33 (2004) 437.
- [12] P.G. Gozzi, *Chem. Soc. Rev.* 33 (2004) 410.
- [13] F. Blank, C. Janiak, *Coord. Chem. Rev.* 253 (2009) 827.
- [14] S.S. Djebbar, B.O. Benali, J.P. Deloume, *Transition Met. Chem.* 23 (1998) 443.
- [15] M.H. Lee, T.V. Giap, S.H. Kim, Y.H. Lee, C. Kang, J.S. Kim, *Chem. Commun.* 46 (2010) 1407.
- [16] N. Nanjundan, R. Narayanasamy, Steven Geib, K. Velmurugan, R. Nandhakumar, M.D. Balakumaran, P.T. Kalaichelvan, *Polyhedron*, 110 (2016) 203.
- [17] CrysAlis, Oxford Diffraction Ltd, Abingdon, U.K. 2006
- [18] O.V. Dolomanov, L.J. Bourhis, R.J. Gildea, J.A.K. Howard, H. Puschmann, *J. Appl. Cryst.* 42 (2009) 339.
- [19] M.J. Frisch, G.W. Trucks, H.B. Schlegel, G.E. Scuseria, M.A. Robb, J.R. Cheeseman, G. Scalmani, V. Barone, B. Mennucci, G.A. Petersson, H. Nakatsuji, M. Caricato, X. Li, H.P. Hratchian, A.F. Izmaylov, J. Bloino, G. Zheng, J.L. Sonnenberg, M. Hada, M. Ehara, K. Toyota, R. Fukuda, J. Hasegawa, M. Ishida, T. Nakajima, Y. Honda, O. Kitao, H. Nakai, T. Vreven, J.A. Montgomery, Jr., J.E. Peralta, F. Ogliaro, M. Bearpark, J.J. Heyd, E. Brothers, K.N. Kudin, V.N. Staroverov, R. Kobayashi, J. Normand, K. Raghavachari, A. Rendell,

- J.C. Burant, S.S. Iyengar, J. Tomasi, M. Cossi, N. Rega, J.M. Millam, M. Klene, J.E. Knox, J.B. Cross, V. Bakken, C. Adamo, J. Jaramillo, R. Gomperts, R.E. Stratmann, O. Yazyev, A.J. Austin, R. Cammi, C. Pomelli, J.W. Ochterski, R.L. Martin, K. Morokuma, V.G. Zakrzewski, G.A. Voth, P. Salvador, J.J. Dannenberg, S. Dapprich, A.D. Daniels, O. Farkas, J.B. Foresman, J.V. Ortiz, J. Cioslowski, D.J. Fox, Gaussian 09, Revision A.02, Gaussian, Inc., Wallingford CT. 2009.
- [20] P. Vijayan, P. Viswanathamurthi, P. Sugumar, M.N. Ponnuswamy, M.D. Balakumaran, P.T. Kalaichelvan, K. Velmurugan, R. Nandhakumar, R.J. Butcher, *Inorg. Chem. Front.* 2 (2015) 620.
- [21] M. Das, R. Nasani, M. Saha, S.M. Mobin and S. Mukhopadhyay, *Dalton Trans.* 44 (2015) 2299.
- [23] P. Seth, L.K.Das, M.G.B.Drew, A. Ghosh, *Eur. J. Inorg. Chem.* 13 (2012) 2232.
- [24] K.S.Banu, T. Chattopadhyay, A. Banerjee, M. Mukherjee, S. Bhattacharya, G.K.Patra, E. Zangrando, D. Das, *Dalton Trans.* (2009) 8755.
- [25] T.J. Mosmann, *J. Immunol. Methods.* 65 (1983) 55.
- [26] M. Blagosklonny, W.S.El-Diery, *Int. J. Cancer.* 67 (1996) 386.
- [27] A. Gohel, M.B. McCarthy, G. Gronowicz, *Endocrinology*, 140 (1999) 5339.
- [28] S. Mukhopadhyay, P.K. Panda, B. Behera, C.K. Das, M.K. Hassan, D.N. Das, N. Sinha, A. Bissoyi, K. Pramanik, T.K. Maiti, S.K. Bhutia, *Food Chem. Toxicol.* 64 (2014) 369.
- [29] M.A. Ali, R. Bose, *J. Inorg. Nucl. Chem.* 39 (1977) 265.
- [30] S.L. Li, J.Y. Wu, Y.P. Tian, Y.W. Tang, M.H. Jiang, H.K. Fun, S. Chantrapromma, *Opt. Mater.* 28 (2006) 897.
- [31] M.A.A.A.A. Islam, M.T.H. Tarafder, M.C. Sheikh, M.A. Alam, E. Zangrando, *Trans. Met. Chem.* 36 (2011) 531.
- [32] M. Yazdanbakhsh, R. Takjoo, *Struct Chem.* 19 (2008) 895.
- [33] K.A. Crouse, K.B. Chew, M.T.H. Tarafder, A. Kasbollah, A.M. Ali, B.M. Yamin, H.K. Fun, *Polyhedron.* 23 (2004) 161.
- [34] P.I.S. Maia, A.G.A. Fernandes, J. Jerley, N. Silva, A.D. Andricopulo, S.S. Lemos, E.S. Lang, U. Abram, V.M. Deflon, *J. Inorg. Biochem.* 104 (2010) 1276.
- [35] D.T. Cromer, J.T. Waber, *The Kynoch Press, Table 2.2B, vol. 4 (1974) Birmingham, England*

- [36] J. Valdez-Martinez, A. Sierra-Romero, C. Alvarez-Toledano, R.A. Toscano, H. Garcia-Tapia, *J. Organomet. Chem.* 352 (1983) 321.
- [37] A. Mohan, P. Sharma, N.K. Jha, *Inorg. Chim. Act.* 106 (1985) 197.
- [38] T. Siang-Guan, A. Show-Hing, T. Soon-Beng, F. Hoong-Kun, K. Khing-Ling, O. Chi-Wi, *J. Chem. Soc. Dalton Trans.* 4 (1997) 465.
- [39] T.B.S.A. Ravooof, K.A. Crouse, M.I.M Tahir, A.R. Cowley, M.A. Ali, *Polyhedron*, 26 (2007) 1159.
- [40] S.S.S. Raj, B.M. Yamin, Y.A. Yossof, M.T.H. Tarafder, H.K. Fun, K.A. Course, *Acta CrystallogrC*, 56 (2000) 1236.
- [41] R. Mattes, H. Weber, *J. Chem. Soc. Dalton Trans.* 3 (1980) 423.
- [42] M.A.F.A. Manan, K.A. Crouse, M.I.M. Tahir, R. Rosli, F.N.F. How, D.J. Watkin, A.M.Z. Slawin, *J. Chem. Crystallogr*, 41 (2011) 1630.
- [43] Tarfder, MTH, Teng-Jen Khoo, KA, A. Course, A.M, Ali, B.M, Yamin, H.K. Fun, *Polyhedron*. 21 (2002) 2691.
- [44] J. Garcia-Tojal, M.K. Urriaga, R. Cortes, L. Lezama, M.I. Arriortua, T. Rojo, *J. Chem. Soc. Dalton Trans.* 15 (1994) 2233.
- [45] T. Koopmans, *Physica*. 1 (1934) 104.
- [46] P.X. Xi, Z.H. Xu, X.H. Liu, F.J. Chen, Z.Z. Zeng, *Chem. Pharm. Bull.* 56 (2008) 541.
- [47] B. Peng, H. Chao, B. Sun, H. Li, F. Gao, L.N. Ji, *J. Inorg. Biochem.* 101 (2007) 404.
- [48] F.J. MegarAlmes, D. Porschke, *Biochemistry*. 32 (1993) 4246.
- [49] S. Dhar, M. Nethaji, A.R. Chakravarty, *J. Inorg. Biochem.* 99 (2005) 805.
- [50] G. Zhao, H. Lin, S. Zhu, H. Sun, Y. Chen, *J. Inorg. Biochem.* 70 (1998) 219.
- [51] A. Zianna, G. Psomas, A. Hatzidimitriou, E. Coutouli–Argyropoulou, M.J. Lalia–Kantouri, *J. Inorg. Biochem.* 127 (2013) 116.
- [52] E. Mrkalić, A. Zianna, G. Psomas, M. Gdaniec, A. Czapik, A. Coutouli–Argyropoulou, M. Lalia–Kantouri, *J. Inorg. Biochem.* 134 (2014) 66.
- [53] D.C. Carter, X. He, S.H. Munson, P.D. Twigg, K.M. Gernert, M.B. Broom, T.Y. Miller, *Science*. 244 (1989) 1195.
- [54] T.N.J.I. Edison, R. Atchudan, J.J. Shim, S. Kalimuthu, B.C. Ahn, Y.R. Lee, *J. Photoch. Photobio. B*. 158 (2016) 235.
- [55] M.R. Eftink, C.A. Ghiron, *Anal. Biochem.* 114 (1981) 199.

- [56] G. Zhao, H. Lin, S. Zhu, H. Sun, Y. Chen, J. Inorg. Biochem. 70 (1998) 219.
- [57] X.Z. Feng, Z. Lin, L.J. Yang, C. Wang, C.L. Bai, Talanta. 47 (1998) 1223.
- [58] H. Gao, L. Lei, J. Liu, K. Qin, X. Chen, Z. Hu, J. Photoch. Photobio. A. 167 (2004) 213.
- [59] R. Loganathan, S. Ramakrishnan, E. Suresh, M. Palaniandavar, A. Riyasdeen, M.A. Akbarsha, Dalton Trans. 43 (2014) 6177.
- [60] M. Ganeshpandian, R. Loganathan, E. Suresh, A. Riyasdeen, M.A. Akbarsha, M. Palaniandavar, Dalton Trans. 43 (2014) 1203.
- [61] I.M. Ghobrial, T.E. Witzig, A.A Adjei, CA: A Cancer J Clin. 55 (2005) 178.
- [62] D.R. Green, S.J. Martin, Curr. Opin. Immuno. 7 (1995) 694.

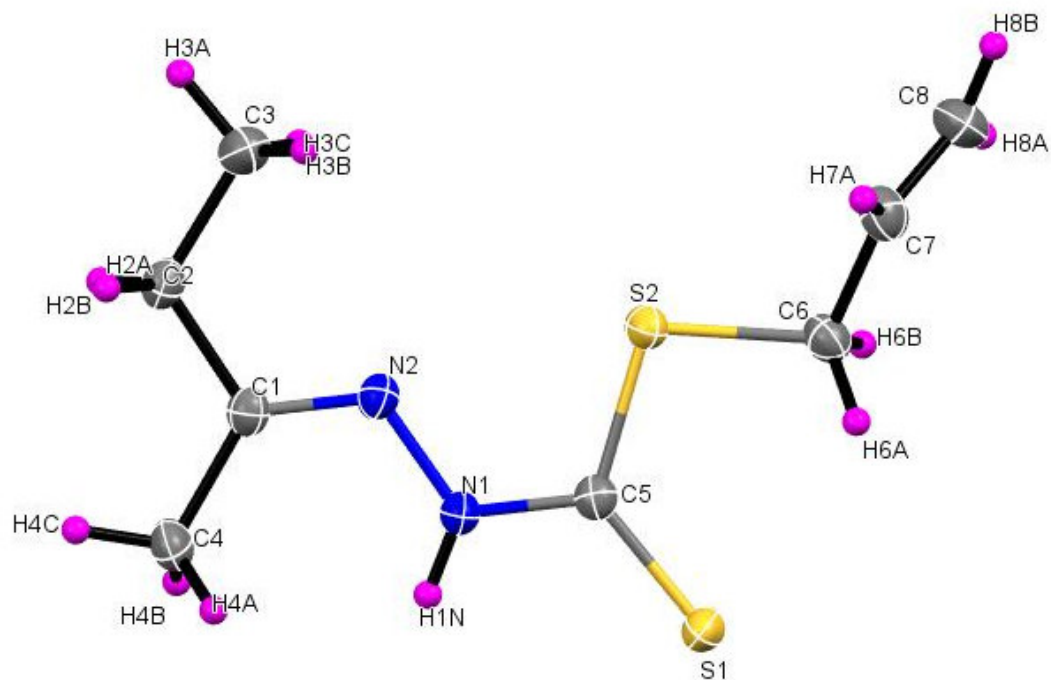


Fig. 1. Molecular structure of [H-emk-sadtc] with 50% probability level.

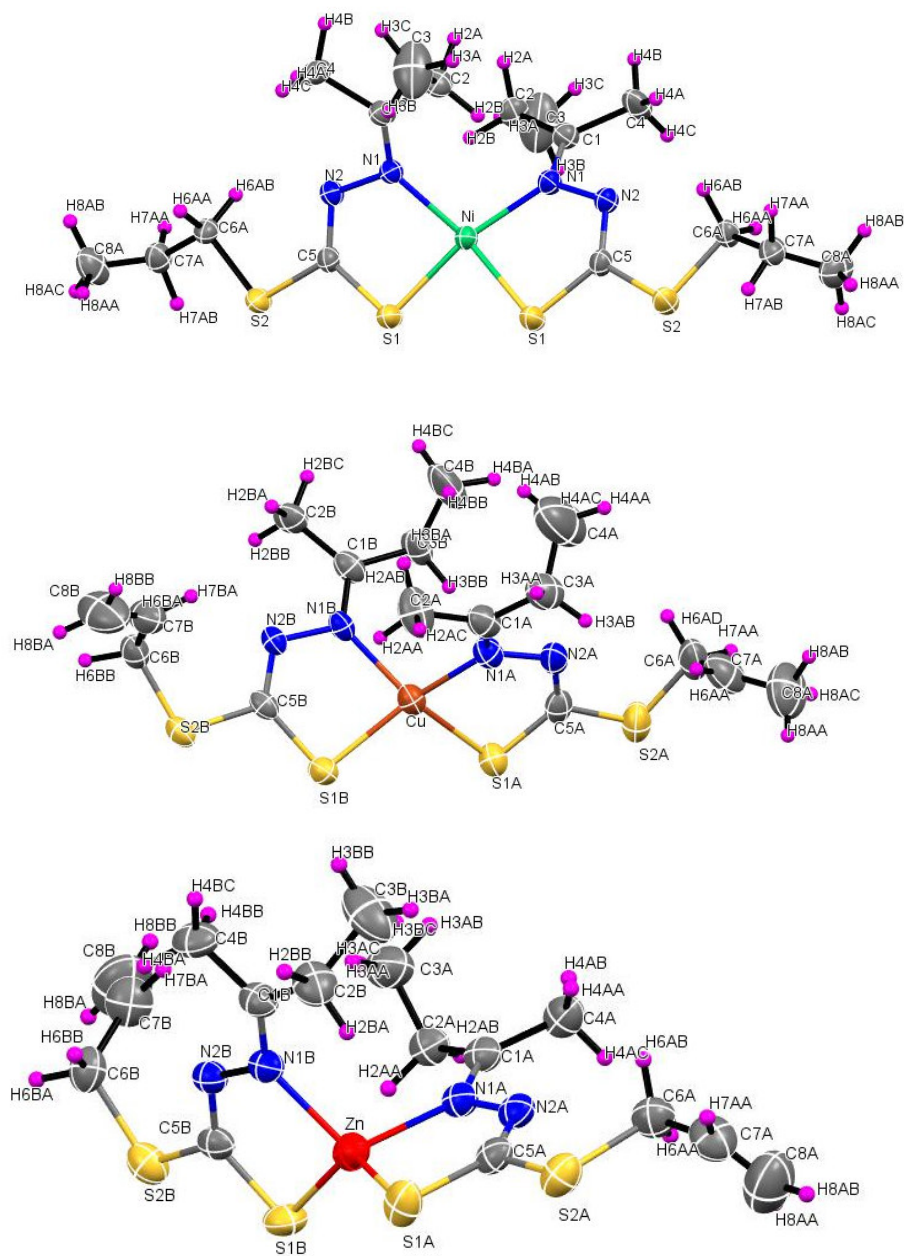


Fig. 2. Perspective view (25% probability ellipsoids) of complexes **1 - 3** with the atom numbering scheme.

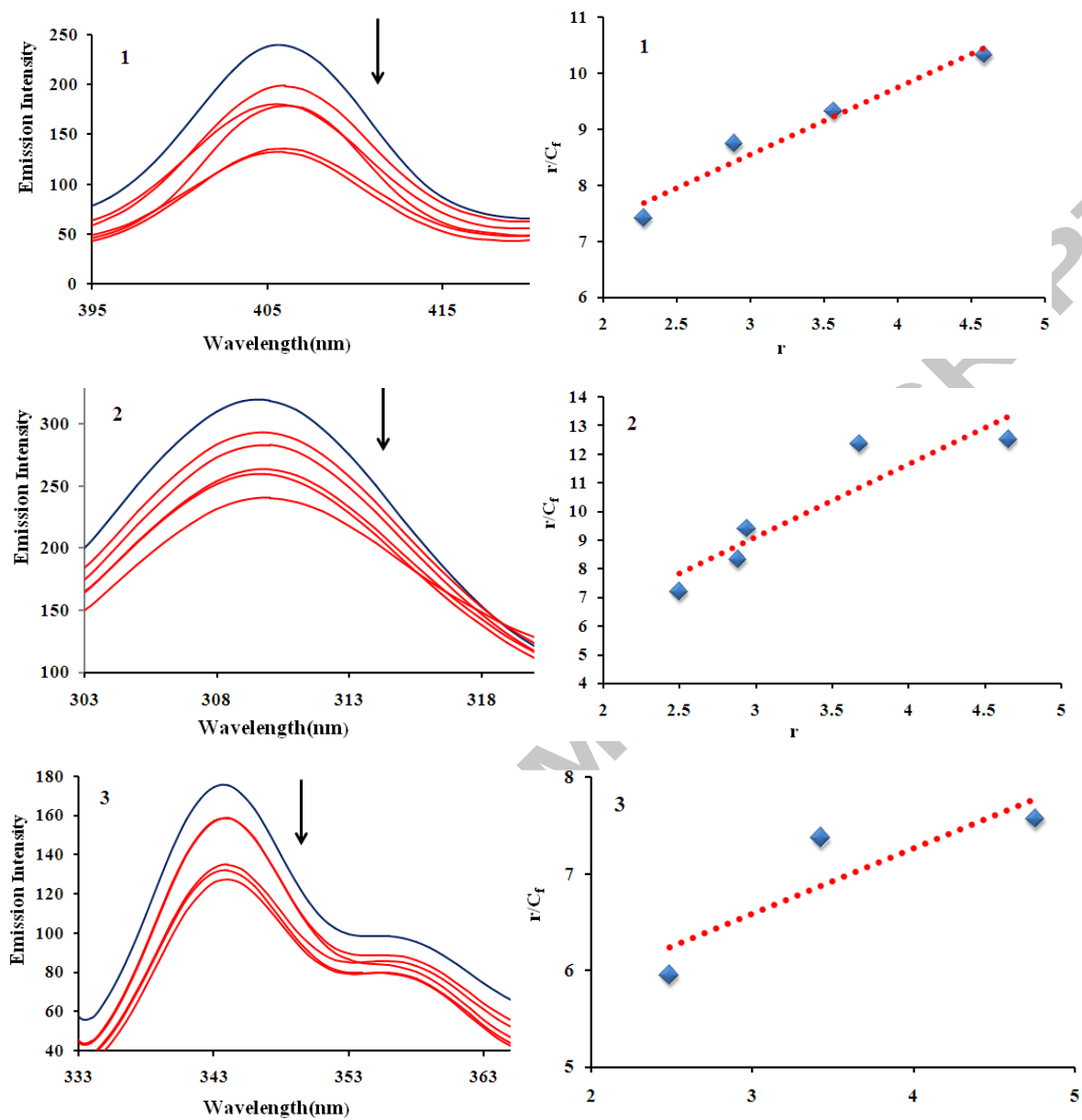


Fig. 3. Emission spectra and Scatchard plots of complexes 1 - 3 (25 μM) in the presence of increasing concentrations of CT - DNA.

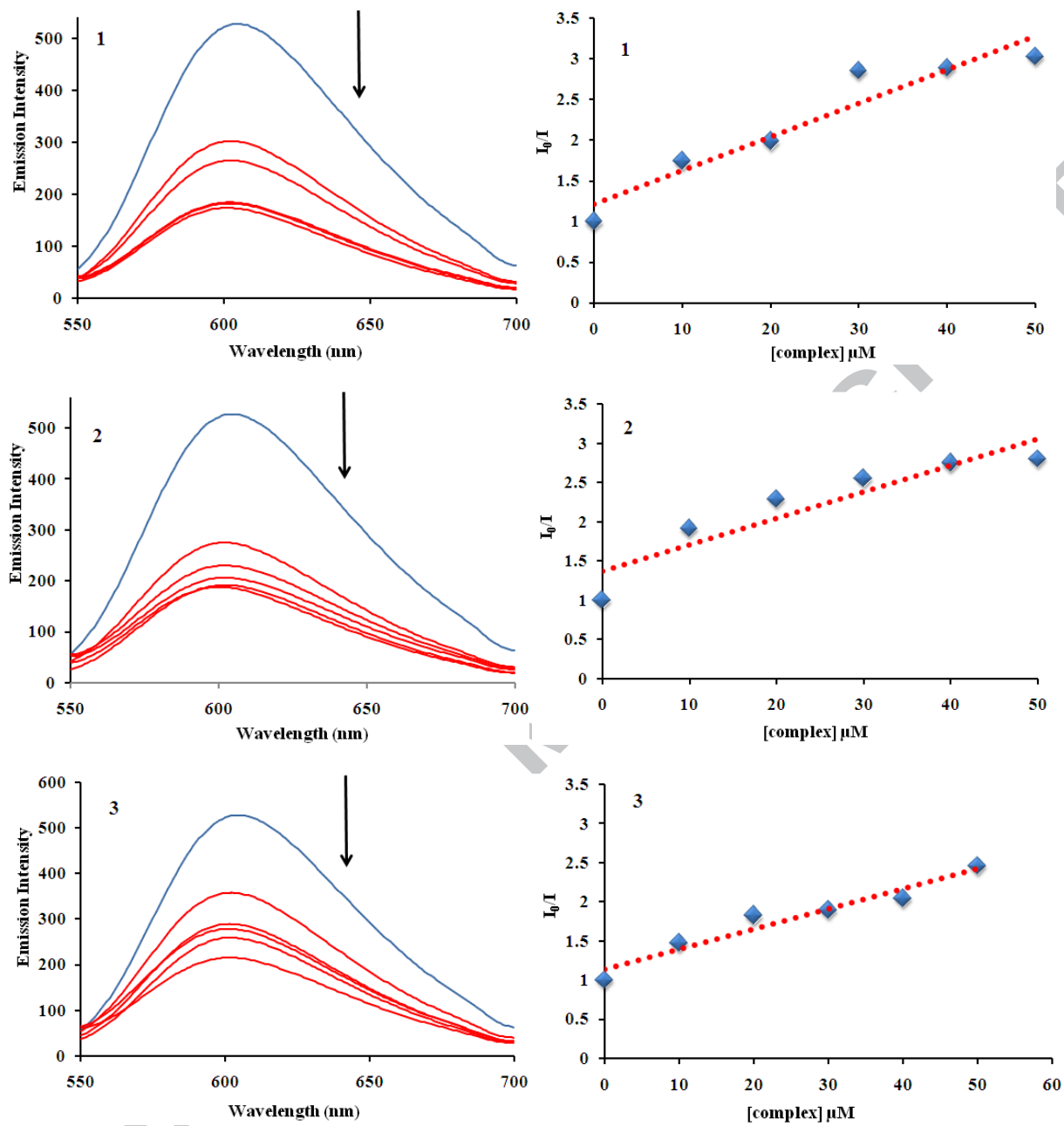


Fig. 4. Fluorescence quenching curves of ethidium bromide bound to DNA: Complexes 1 – 3.

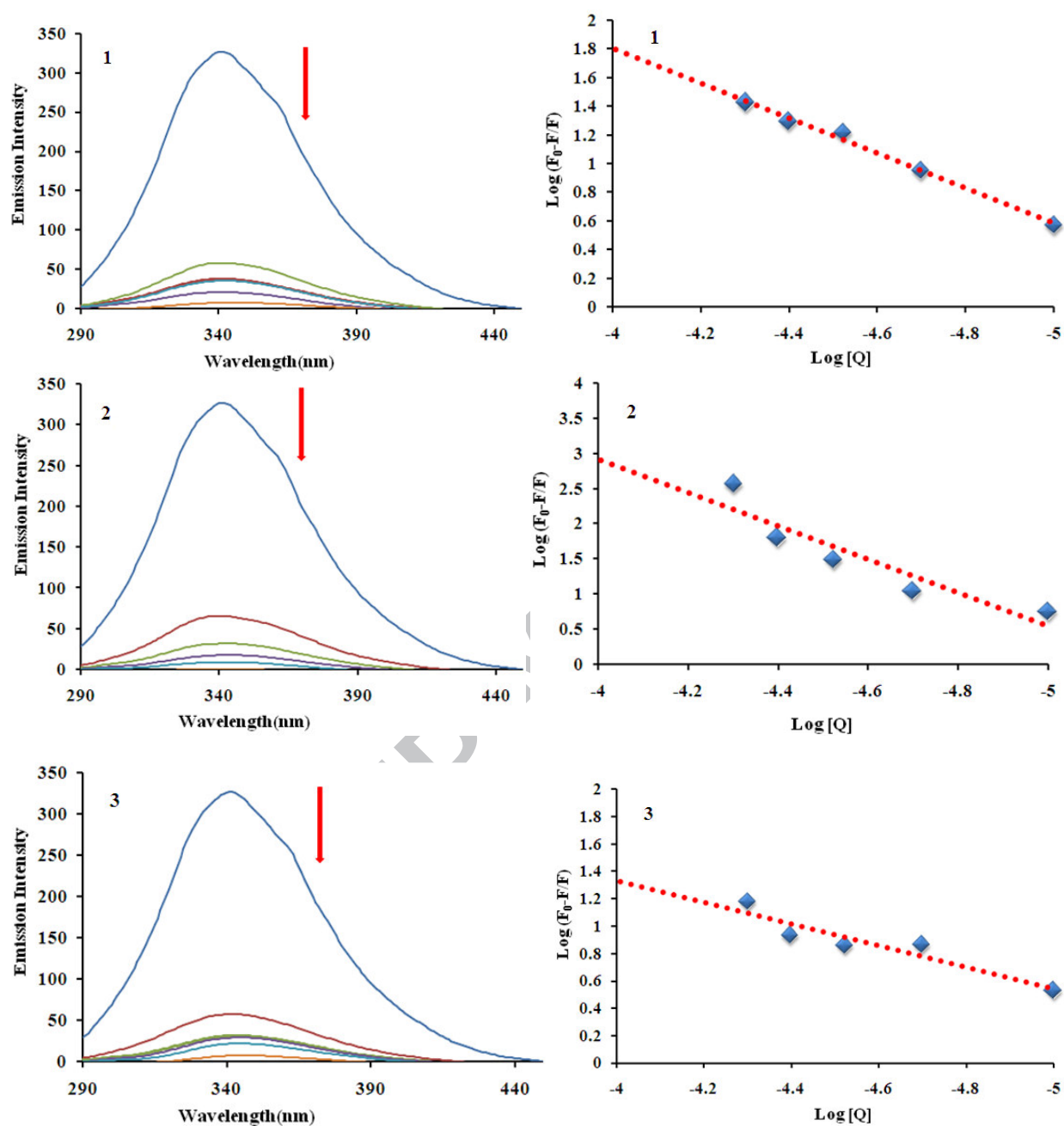


Fig . 5. Emissive spectra and Stern–Volmer plots of BSA upon the titration of complexes **1 - 3**. The arrow shows change upon increasing complex concentration.

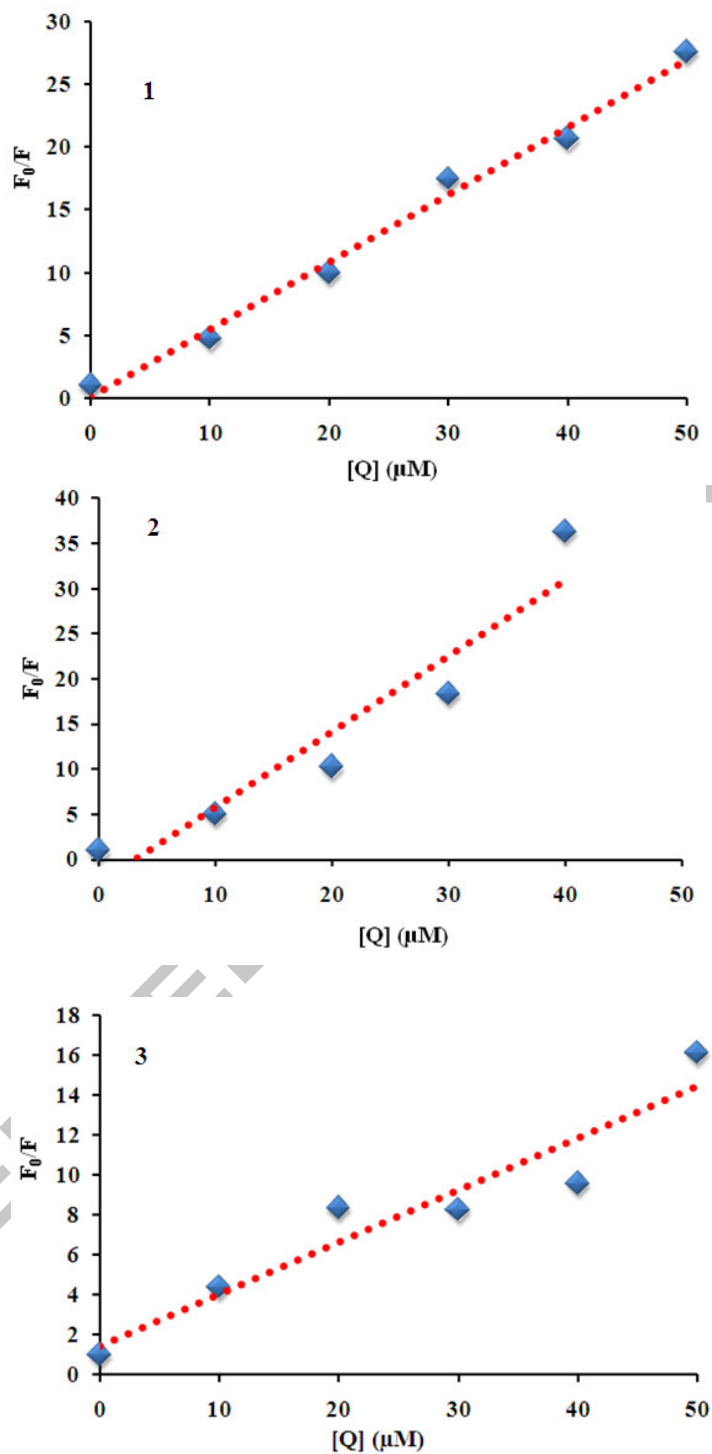


Fig. 6. Scatchard plots of complexes 1 – 3.

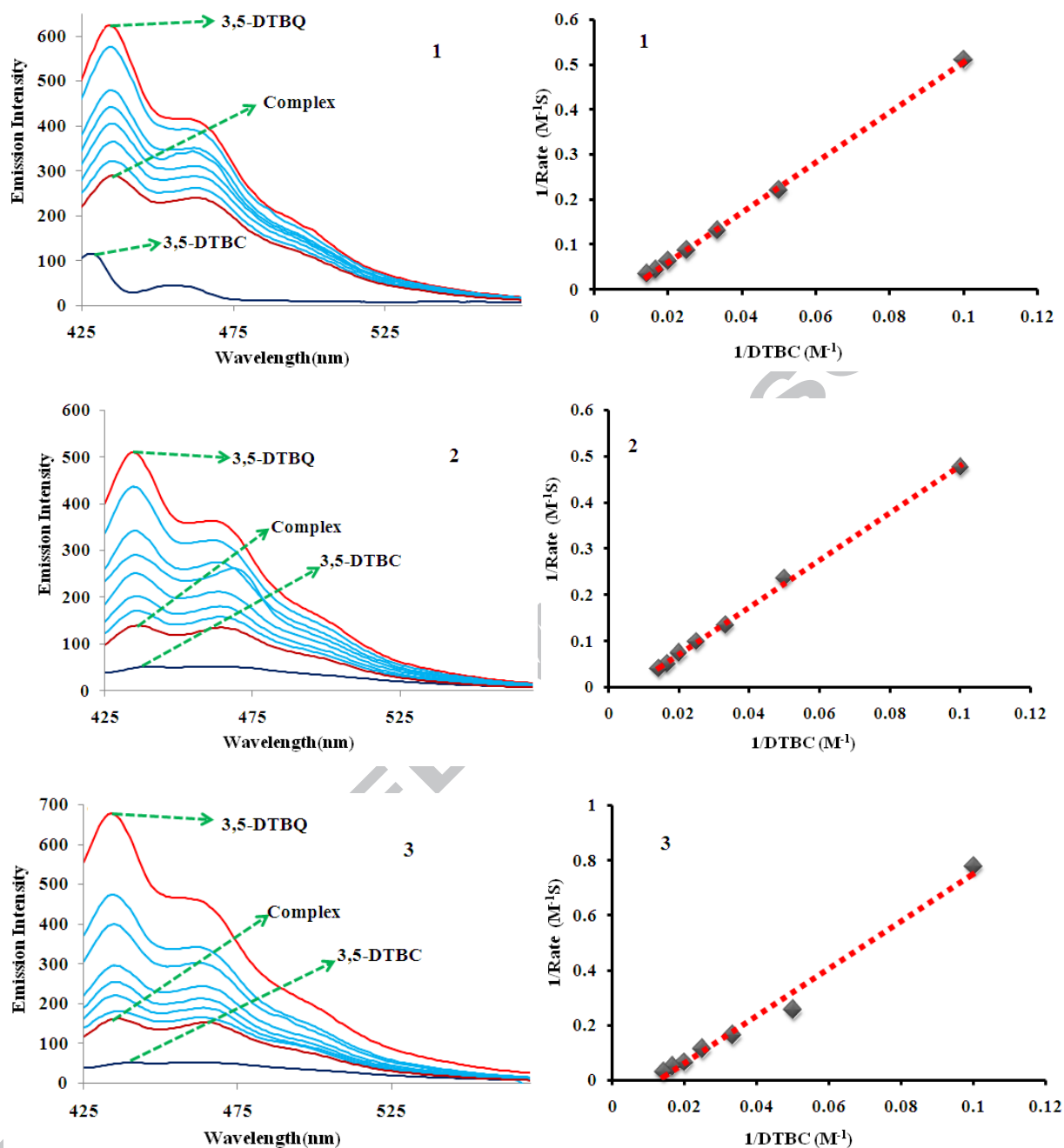


Fig. 7. Increase in emission after addition of 3,5 - DTBC to DMSO containing complexes **1 - 3** (10^{-4} M). The spectra were recorded at every 15 min interval.

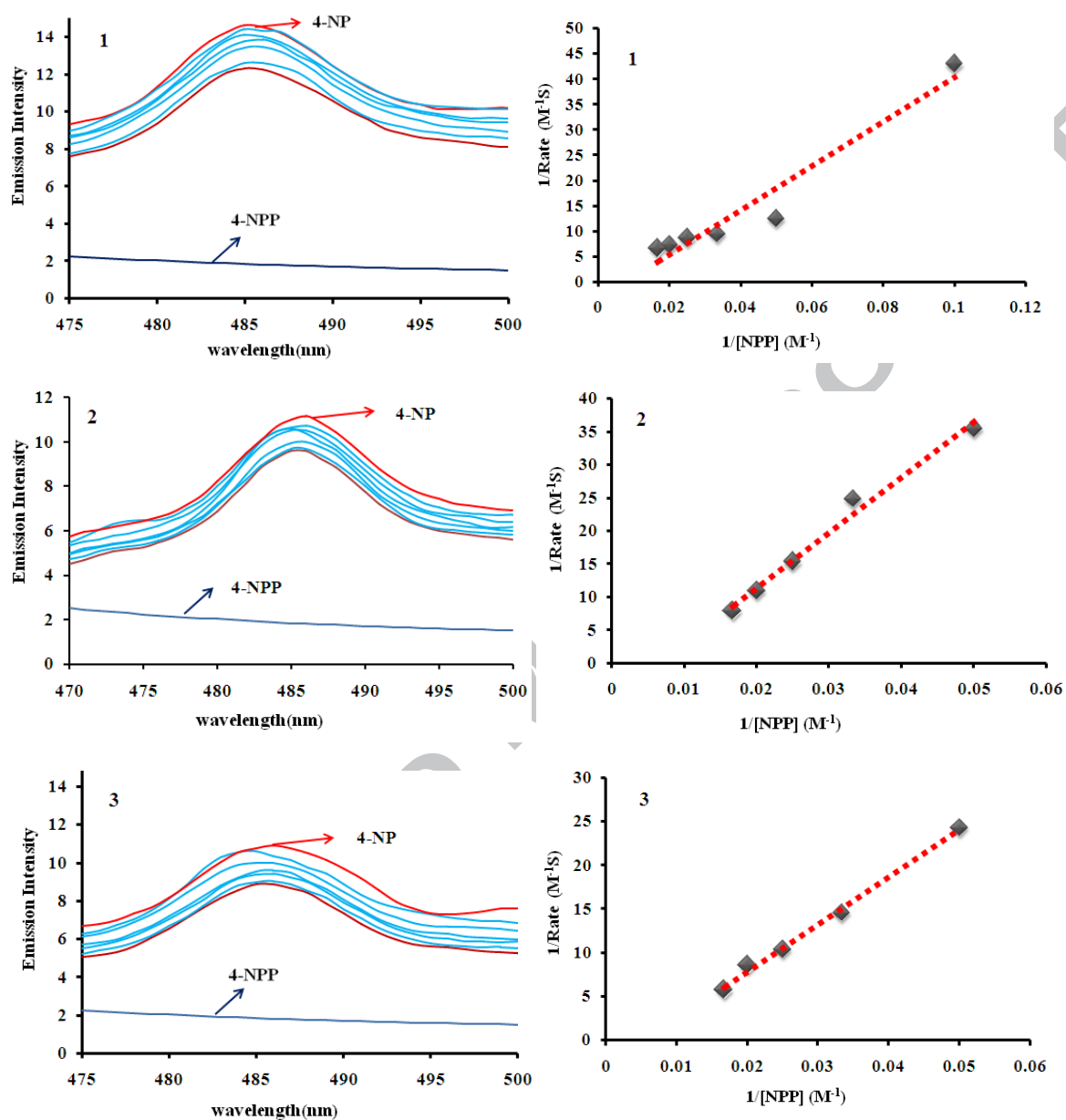


Fig. 8. Increase in emission after the addition of 4 – NPP to DMSO containing complexes 1 - 3. The spectra were recorded at every 15 mins interval.

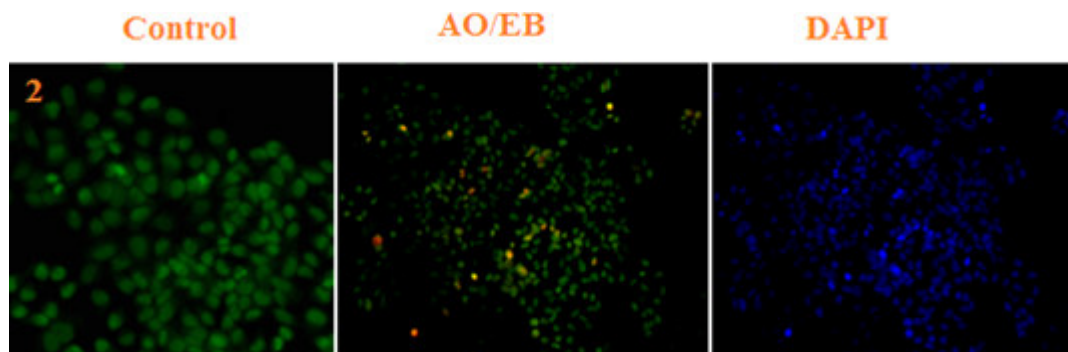


Fig.9. *In vitro* fluorescence images of HeLa cancer cells after AO/EB and DAPI staining incubated 24 hr treatment of complexes (1-3) with fixed concentrations.

Table 1Crystal data and structure refinement for ligand and its complex **1-3**.

	[H-emk-sadtc]	1	2	3
Chemical formula	C ₈ H ₁₄ N ₂ S ₂	C ₁₆ H ₂₆ N ₄ NiS ₄	C ₁₆ H ₂₆ CuN ₄ S ₄	C ₁₆ H ₂₆ N ₄ S ₄ Zn
Wavelength	0.71073 Å	0.71073 Å	0.71073 Å	0.71073 Å
Crystal system	Monoclinic	Monoclinic	orthorhombic	Triclinic
Space group	P 21/c	I 2/a	P 21/c	P -1
a (Å)	5.0872(3)	14.3214(16)	11.0401(8)	9.0734(5)
b (Å)	14.5283(9)	7.6049(8)	17.6150(14)	11.1542(7)
c (Å)	14.5727(7)	20.1891(19)	12.3177(10)	12.3637(5)
α (°)	90	90	90	109.604(5)
β (°)	98.454(5)	93.060(10)	110.672(8)	92.681(4)
γ (°)	90	90	90	103.294(5)
Volume Å ³	1065.34(11)	2195.7(4)	2241.2(3)	1136.64(11)
Z	4	4	2	2
Density (cal) g/cm ³	1.261	1.408	1.385	1.367
Absorption coefficient mm ⁻¹	0.452	1.271	1.354	1.455
F(000)	432	984	976	488
Theta range for data collection	3.983 to 32.840°	3.404 to 32.571°	3.288 to 32.732°	3.384 to 32.835°
Index ranges	-7<=h<=4, -20<=k<=21, -20<=l<=21	-20<=h<=21, -10<=k<=10, -26<=l<=29,	-15<=h<=16, -24<=k<=26 -18<=l<=17,	-13<=h<=13, -9<=k<=16, -18<=l<=18
Reflections collected	7452	7747	17373	13681
Independent reflections	3551 [R(int) = 0.0328]	3569 [R(int) = 0.0343]	7390 [R(int) = 0.0588]	7495 [R(int) = 0.0322]
Absorption correction	Semi-empirical from equivalents	Semi-empirical from equivalents	Semi-empirical from equivalents	Semi-empirical from equivalents
Max. and min. transmission	1.00000 and 0.84942	1.00000 and 0.77358	1.00000 and 0.00736	1.00000 and 0.63433
Refinement method	Full-matrix least-squares on F ²	Full-matrix least-squares on F ²	Full-matrix least-squares on F ²	Full-matrix least-squares on F ²
Goodness-of-fit on F ²	1.102	1.069	1.049	1.011
Data / restraints / parameters	3551 / 21 / 143	3569 / 21 / 128	7390 / 30 / 242	7495 / 117 / 265
Final R indices data; I>2σ(I)	R1 = 0.0470, wR2 = 0.1014	R1 = 0.0574, wR2 = 0.1382	R1 = 0.0985 wR2 = 0.1437	R1 = 0.0635, R2 = 0.01409
R indices (all data)	R1 = 0.0706, wR2 = 0.1130	R1 = 0.0837, wR2 = 0.1587	R1 = 0.1962, wR2 = 0.1907	R1 = 0.1356, wR2 = 0.1856

Table 2Selected bond lengths (Å) and bond angles (°) of [H-*emk-sadtc*] and its complexes **1-3**.

Bond length(A°)	[H- <i>emk-sadtc</i>]	Bond length (A°)	1	2	3
S(1)-C(5)	1.6603(17)	M-N	1.948(2)	1.987(4), 1.996(5)	2.040(3), 2.053(3)
N(1)-N(2)	1.3865(19)	M-S	2.1545(9)	2.2291(16) , 2.2345(19)	2.2650(14), 2.2752(13)
N(1)-C(5)	1.338(2)	N-N	1.430(3)	1.411(6), 1.406(5)	1.407(5), 1.402(4)
Bond angles(°)		Bond angles(°)			
C(5)-S(2)-C(6)	102.7(3)	<i>Cis</i> N-M-S	86.10(7)	86.16(12), 85.77(15)	87.51(10), 87.27(10)
C(5)-N(1)-N(2)	118.34(14)	<i>Trans</i> N-M-S	161.89(8)	145.24(15) , 145.91(13)	122.81(9), 126.90(9)
C(5)-N(1)-H(1N)	117.9(14)	N-M-N	104.51(14)	103.19(19)	108.41(12)
N(2)-N(1)-H(1N)	123.5(14)	S-M-S	87.76(5)	105.22(7)	126.47(5)

Table 3

Emission spectral properties of complexes **1 - 3** bound to calf thymus DNA.

Complexes	K_{sv} (10^4 M^{-1})	K_b (10^5 M^{-1})	K_{app} (10^5 M^{-1})
1	2.9	1.97	1.60
2	3.2	2.556	1.74
3	2.3	0.675	1.59

Table 4

Stern-volmer quenching constant (K_{sv}), Quenching rate constant (K_q), Protein binding constant (K_b) were determined by fluorescence spectra and 'n' is the number of binding sites per BSA.

Complex	$K_{sv} (M^{-1})$	$K_q (M^{-1})$	$K_b (M^{-1})$	n
1	3.51×10^5	3.51×10^{13}	2.6×10^6	1.16
2	4.6×10^5	4.6×10^{13}	1.6×10^7	1.3
3	3.59×10^5	3.59×10^{13}	1.9×10^4	0.72

Table 5Kinetic parameters for catecholase activity of complexes **1 – 3**.

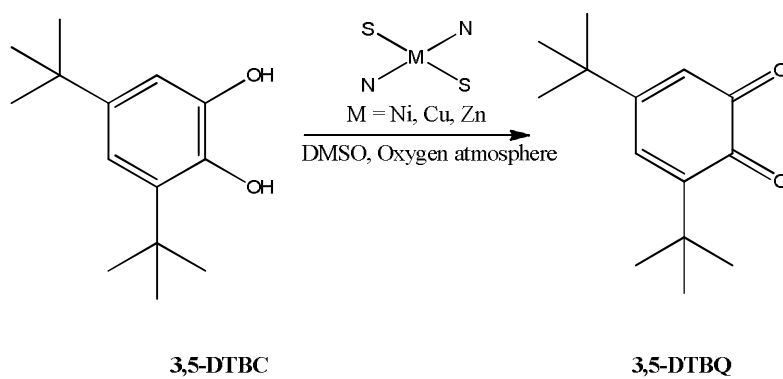
Complex	$K_m(10^{-4}M)$	$V_{max}(10^{-4}MS^{-1})$	$K_{cat}(h^{-1})$
1	76.5	8.84	76.5
2	111	20	111
3	75.3	5.74	75.3

Table 6Kinetic parameters for Phosphatase activity of complexes **1 – 3**.

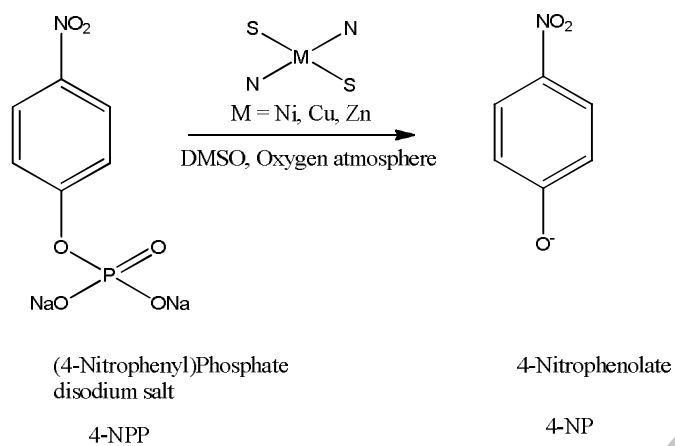
Complex	$K_m(10^{-3}M)$	$V_{max}(10^{-3}MS^{-1})$	$K_{cat}(h^{-1})$
1	153	0.183	3076
2	178	0.307	3579
3	132	0.304	2657

Table 7*In vitro* cytotoxicity of the complexes in normal and cancer cell lines

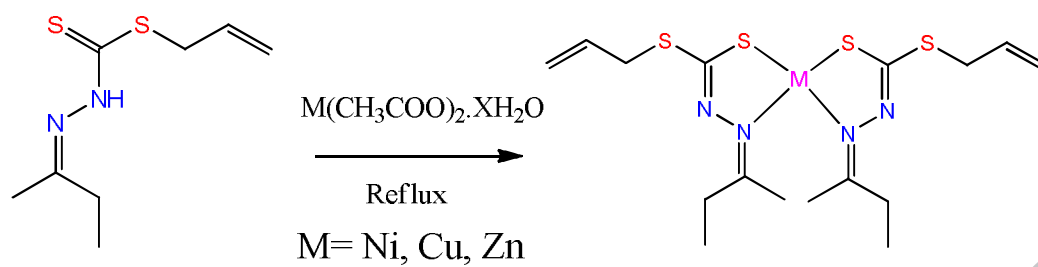
Compound	IC ₅₀ (μ M) ^a	
	Vero	HeLa
1	65.51 \pm 3.41	37.74 \pm 1.59
2	60.86 \pm 2.65	35.34 \pm 2.03
3	72.75 \pm 1.79	45.32 \pm 1.02
Cisplatin	-	35.7 \pm 0.0850



Scheme 1. Schematic depiction of 3,5 - DTBC catalyzed by Schiff base metal complexes **1 - 3**.



Scheme 2. Schematic depiction of the hydrolytic reaction of 4 - NPP by the complexes **1 - 3**.

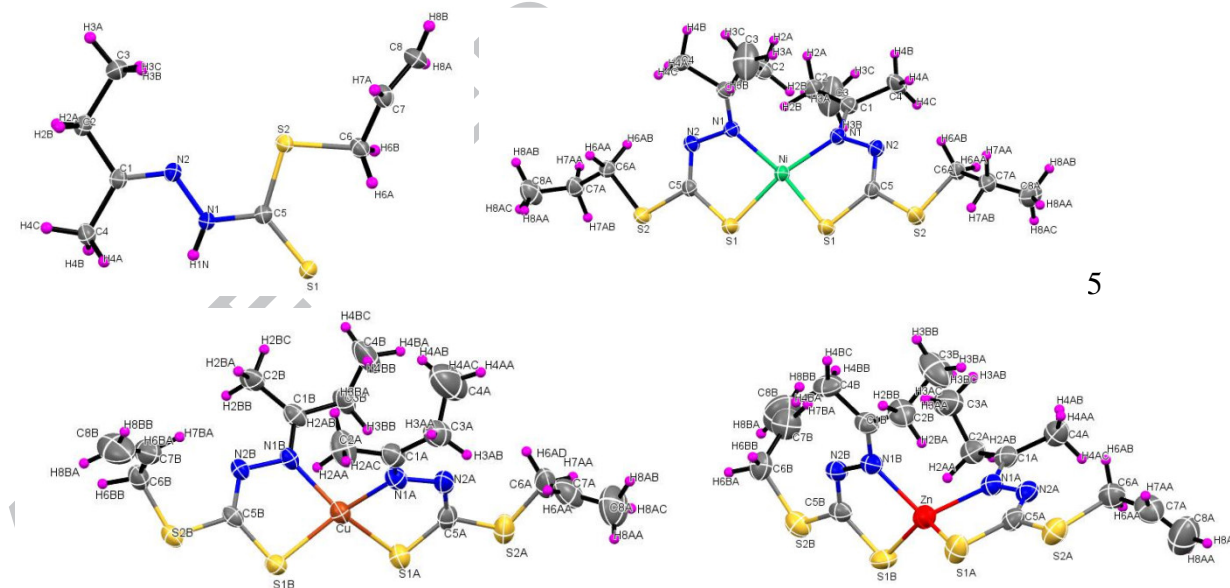


Scheme 3. Synthesis of complexes **1 – 3**.

Graphical Abstract Synopsis:

Bidentate Schiff - base ligand [**H-emk-sadtc**] and its Ni(II), Cu(II) and Zn(II) complexes were synthesized. Single crystal XRD studies revealed that all the complexes have distorted square planar geometry. DNA and BSA binding studies were displayed. Complexes were exhibit excellent catecholase and Phosphatase hydrolysis activity. Cytotoxicity in the low μM range was found for all complexes.

Graphical Abstract Pictogram:



5

Highlights

- Dithiocarbazate Schiff base complexes have been synthesized.
- They have been characterized by experimental and computational techniques.
- CT-DNA and BSA binding affinity were studied.
- Catecholase and Phosphatase activity were studied.
- *In vitro* cytotoxicity evaluation of the complexes.